2015-01-01

Design Optimization And Optical Characterization Of A High Temperature Solar Receiver

Samia Afrin
University of Texas at El Paso, samia_afrin@yahoo.com

DESIGN OPTIMIZATION AND OPTICAL CHARACTERIZATION OF A HIGH TEMPERATURE SOLAR RECEIVER

SAMIA AFRIN

Doctoral Program in Environmental Science & Engineering

APPROVED:

Vinod Kumar, Ph.D., Chair

Zhiwen Ma, Ph.D.

Norman D Love, Ph.D.

Vivek Tandon, Ph.D.

Charles Ambler, Ph.D.
Dean of the Graduate School

Dedication

To my parents,
For teaching me the joy of learning,
The importance of education,
And preparing me for life after childhood

To my dear friend Mahamud for being supportive all the way

And

To all of my friends and family

For supporting and encouraging me through the past years

DESIGN OPTIMIZATION AND OPTICAL CHARACTERIZATION OF A HIGH TEMPERATURE SOLAR RECEIVER

by

SAMIA AFRIN, MS

DISSERTATION

Presented to the Faculty of the Graduate School of

The University of Texas at El Paso

in Partial Fulfillment

of the Requirements

for the Degree of

DOCTOR OF PHILOSOPHY

Department of Environmental Science and Engineering

THE UNIVERSITY OF TEXAS AT EL PASO

December 2015

Acknowledgements

I would like to thank everyone who has helped and supported me in this endeavor. I am grateful to my advisor Vinod Kumar for his continuous support and encouragement. His guidance has helped me maintain a broader perspective of my graduate education and discover my independence and competence. I would also like to thank Dr. Zhiwen Ma and Dr. Clifford K. Ho for providing me the opportunity to work with these world class National Labs; National renewable Energy Laboratory and Sandia National Laboratories. They gave me the opportunity to select this incredible and exciting dissertation topic and become supportive mentor and dedicated advisor to me. Additionally I thank the Thermal Systems Group at NREL especially Mark Mehos, Janna Martinek, Judith Gomez, Judy netter, Tim Wendlin, Guangdong Zhu and Terry Spinuzzi. This dissertation would not exist without their countless effort by developing the test field and contributing to every aspect of this project. Thank you all of my committee members Dr. Vinod Kumar, Dr. Zhiwen Ma, Dr. Clifford K. Ho and Dr. Norman Love for their time supporting, guiding and evaluating this work. Finally I would like to thank my family my friends and all fellows who support me throughout my work.

This work was sponsored by National Renewable Energy Laboratory under the award ZGG-5-52122-01which is granted by the U.S. Department of Energy award no. DE-EE0001586.

Abstract

Concentrated solar power (CSP) is a fast forwarding technology in power generation sector because of its' competitive price, abundance in nature and the most important fact is its' energy storage capability. Among the four types of available CSP technology, central receiver has more potential concerning with high temperature, power block efficiency and levelized cost of energy (LCOE). Other than conventional type of receiver design, the concept of this work is very particular in a sense of its design novelty.

National Renewable Energy Laboratory (NREL) come up with a new concept of high temperature solar receiver called near black body (NBB) receiver. This receiver design requires high specular reflective surface in its' front section at operating temperature 150^{o}C. High specular reflective surface refers to mirror finished surface. However, this specular reflective surface application is for high temperature solar receiver, the surface needs to be durable from thermal cycling, oxidation and environmental effect. This mirror finished specular surface helps to penetrate the sunlight inside the hollow tube and hence increase receiver's efficiency. But at such operating temperature and environmental condition, optical properties degradation rate is high. So to protect this mirror surface a thin layer of SiO_2 has been deposited by sol-gel method on top of electroplated silver coating. To obtain a rigid thin film structure, sol-gel procedure has been tested extensively by varying most dominant sol-gel parameters. Endurance test has been performed in the furnace at 150^{o}C for 1000 hours.

Table of Contents

List of Tables

List of Figures

Chapter 1: Introduction

1.1 CONCENTRATING SOLAR POWER

The limited supply of fossil fuel, the adverse impact of greenhouse emission on the global environment and the growing concern of climate change dictate the arising usage of renewable energy sources. Concentrated solar power (CSP) is the most potential renewable source of energy for solar to thermal or electric conversion because of its abundant resource. It satisfies most of the environmental issue as there is a small pollution compare to the coal power plant while generating electricity. Solar technology has a strong potential to meet our growing demand of energy and reduce dependence on fossil fuels. The amount of energy being consumed by us is only of energy being intercepted by earth [1].

Now-a-days CSP is a fast forwarding technology in power generation sector because of its concern to the climate change issues. 1 magawatt (MW) CSP plant is capable to abstain 688 tons of CO_2 emission compared to combined cycle system and 1360 tons of CO_2 emission if comparable with coal/steam cycle power plant [2]. 2014 CSP roadmap envisions that by 2050 global installed CSP capacity will reach to 1000 GW which would be capable to replace 2.1 gigatonnes (Gt) of CO_2 emissions annually [3].

The first commercial power plant, Solar One has been developed in 1982, California, USA [4]. This 10 MWe capacity plant was decommissioned in 1988 and retrofitted as a solar power tower utility-led project. This Solar Two CSP power plant was the first solar power tower commercially launched technology. It was in operation for only three years (1996-1998) but the objective was to demonstrate the economic possibility of commercial CSP tower technology [5]. Since then this trend is elevating and at the end of first decade of 21st century 1.3 GW of CSP plants are in operation worldwide. As of 2014, more than 4700 MW CSP plants are in operation

[6]. These plants are mainly owned by USA and Spain, however, North Africa, Middle East, India and China all are investing on CSP technology.

Four types of CSP technologies are accessible these days, i.e. parabolic trough, linier Fresnel, sterling dish and solar power tower. Among them solar power tower or central receiver CSP technology has more potential concerning with high temperature, power block efficiency and levelized cost of energy (LCOE) [7]. Here, incident sun rays hits the mirror surface called heliostats and reflected back towards a high temperature receiver where the concentrated rays transfer the heat energy to the heat transfer fluid (HTF). Concentrated solar flux impinging on the receiver allow the HTF to reach about 1000^{o}C temperature and then integrate this thermal energy into more efficient thermodynamic cycles for solar to electric power conversion.

In central receiver, the performance requirements of the plant are evaluated on three major subsystems: collector, receiver and power conversion subsystems [8]. The US department of Energy pursue for advanced receiver design under SunShot initiative to come across higher efficiency thermodynamic power cycles that can efficiently convert thermal-to-electric power with greater than 50% efficiency. The conventional design includes an array of tubes with multiple panels form a cylindrical shape. Working fluid passes through the tubes from inlet port and moving towards to outlet after receiving incident concentrated sunlight on the receiver's tube wall [9]. This typical design is known as external tubular receiver.

The SunShot initiative program set a subsidy-fee levelized cost of energy (LCOE) goal for CSP which will provide electricity at a cost of $0.06/kWh or less by the end of the decade. Figure 1.0.1 is a graphical presentation which shows the transformation of cost reduction of four prime subsystems of solar tower. Price is moving downward since 2010 ($0/21/kWh) because of significant technical advances in performance and efficiency. In general, this target requires higher operating temperature for longer lifetime which drives higher efficiency and lower cost.

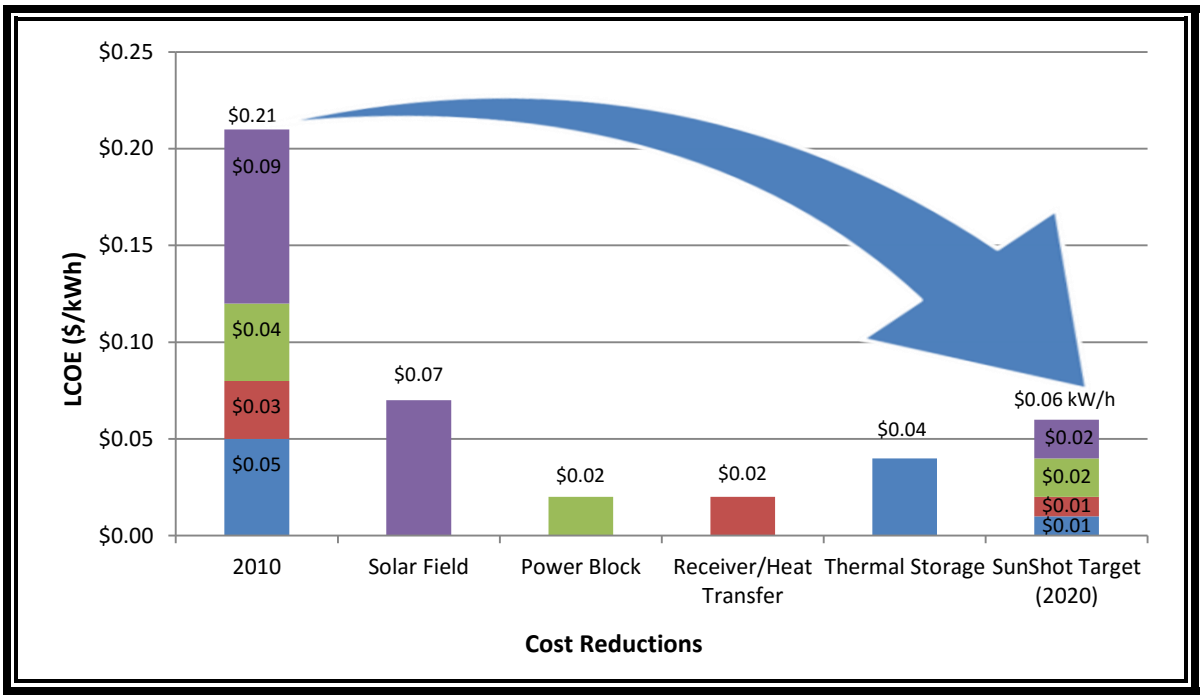

Figure1.1: Department of Energy SunShot goal 2020 [10]

1.2 HIGH TEMPERATURE SOLAR TOWER RECEIVER

Power generation from renewable sources has limitations; like, intermittency, remoteness of good resource regions, and scale potential. Central receiver technology has promising approaches to address these issues. This is why this technique is considered as one of the big shot in power generation sector. Todays' central solar receiver technologies can reach up to 1000°C which satisfy receiver's efficiency target (≥50%) by mitigating high temperature stability challenge (>650°C).

Todays' central solar receiver technologies can reach up to 600°C using either steam or molten nitrate salt as the heat transfer fluid (HTF). Above 600°C, molten nitrate salt becomes unstable while operating with Rankine power cycle and can reach ~35% efficiency [11]. As because of this limitation, power tower technology can't reach <1000°C even though it has the capability. To solve this issue, new type of HTF is proposed accompanying with different type of receiver and thermodynamic cycle. The concept of closed Brayton cycle with supercritical CO_2 as

the working fluid first proposed in 1968, by Feher [12]. This concept is widely used on nuclear power generation in gas reactors and then also explored in solar power plants [8, 13-16].

In parallel with supercritical CO_2 extensive research is going on solid particle receiver (SPR). This is a direct absorption tower receiver idea first came out in 1980 [17]. Benefits of this receiver is the HTF can also be used as thermal energy storage (TES) medium which is a very economical way to meet the SunShot goal of $0.06/kWh. The two pioneer national laboratories; Sandia National Laboratories in Albuquerque, NM and National Renewable Energy Laboratory in Golden, CO, are working together to test their own prototype receiver in a solar field [18, 19].

Dr. Zhiwen Ma, senior scientist from NREL received $3.7M grant for his novel near-blackbody high temperature concept [19]. The overall purpose of this project is to implement a research project that can investigate, develop and test the near black-body high temperature solid particle receiver and examine different modes of heat transfer mechanism in gas-solid particle system at high temperature (1000+ ^oC). Design objective is to overcome the issues associated with current molten salt CSP system i.e. heat transfer fluid (HTF) instability at <600^oC, high efficiency and cost barriers.

The novelty of this conceptual NBB receiver is, this design is divided into three different optical zones; front or flare section, middle section and end section. These three sections are distinguished by their optical properties and thermal stability at temperatures. That is, flare section is highly specular surface but operable only at 150^oC, middle section is high hemispherical but low specular reflective surface which can thermally stable up to 1000^{o}c and the end section is an oxidized metallic surface with 95% absorptivity at 1000^{o}c.

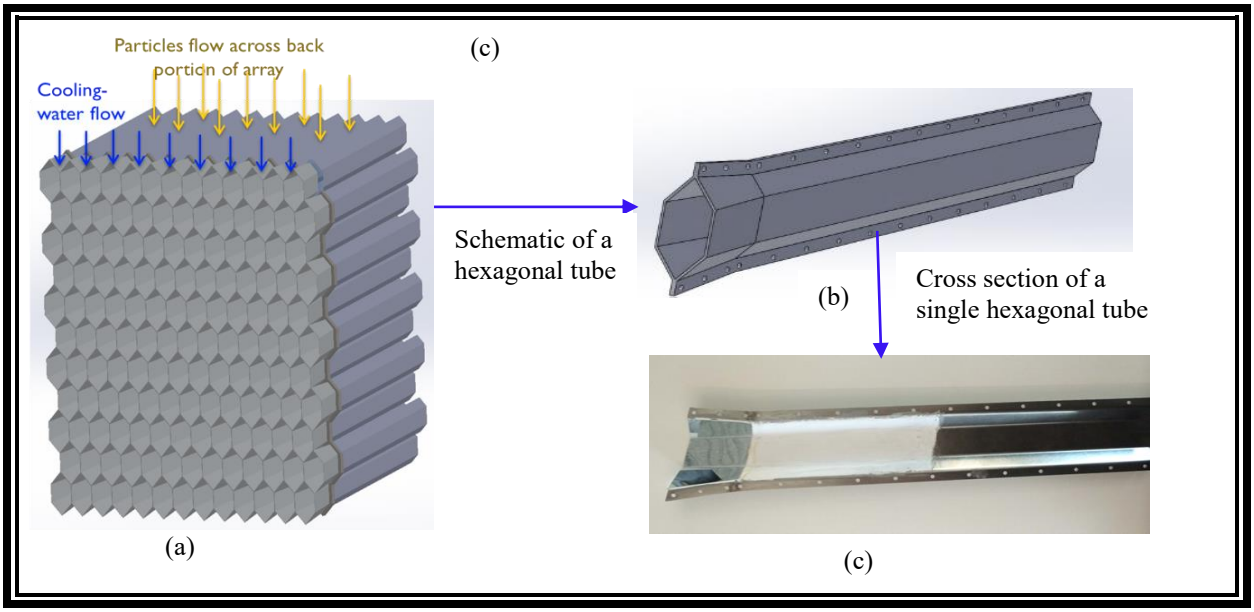

Figure 1.2: (a) Schematic of a NBB receiver (b) Schematic of a single hexagonal tube (c) Cross section of a hexagonal tube

Figure 1.2(a) is a schematic diagram of a small prototype NBB receiver and 1.2(b), (c) are a close shot of single hexagonal tube. 1.2(c) is cross sectional view of a fabricated tube with three different reflective surface. Fabrication procedure and on-sun testing of this single tube is discussed in details in chapter 4.

In this thesis I concentrate on optical characterization of NBB receiver. This receiver design requires high specular reflective surface in its' front section at operating temperature 150°C. This mirror finished specular surface helps to penetrate the sunlight inside the hollow tube and hence increase receiver's efficiency. But at such operating temperature and environmental condition, optical properties degradation rate is high. Most commonly used mirror finished high specular reflective material is silver (Ag) or Aluminum (Al) [20]. But the degradation rate under ambient conditions without a protection layer is rapid for both materials. Unprotected silver surfaces tend to degrade in ambient air, especially at elevated temperatures. Al is not a very good option to use because of its ability to scratch while handling. Real solar field is located in a very

harsh weather condition and it may also degrade its specularity significantly during cleaning and handling [21].

For practical reflective surface formation, a protective, transparent top coating can be applied to provide a barrier to oxygen and to limit the coating degradation. Coating development and degradation rate test is time consuming, risky and uncertain. To alleviate the development risk, two approaches were adapted: first searched existing coating methods and examined their applicability to the receiver requirements; second, modify within the available applicable coatings, so as to accelerate the coating application to the receiver. Candidate coating materials are studied and reviewed extensively and chemical stability investigated from practical application and preliminary thermodynamic modeling. Discussed with several coating expertise including electroplating, sol-gel coating, Alanod MIRO-SUN® reflector, ceramic coatings, and high-temperature paints, to leverage the existing industry coating experiences to accelerate the technology development and to minimize the implementation risk.

1.3 OVERVIEW

In chapter 2, a broad literature review has done on high specular reflective materials, use of ceramic paint as a diffusive coating and its application at very high temperature. Possible coating options are discussed based on its current use and expertise comments. Also present a very specific discussion on HTF, thermodynamic cycle and how these parameters rule on overall efficiency of a solar power plant.

In chapter 3, following a brief introduction to the different type coating method, pros and cons of available coating options. A preliminary test plan which was executed based on literature survey of specular reflective materials. Instruments used in this experiment and measuring devices are outlined in a table.

In chapter 4, the governing equations for fluid flow and radiation model are discussed. A thermochemical software HSC chemistry is introduced in this chapter which was used to calculate

possible chemical reaction happen at high temperature. Another simulator SolTrace modeling software for solar field flux distribution calculation is studied here.

In chapter 5, sol-gel coating scope, effective parameters of sol-gel preparation, methodology and testing condition are presented in details. Samples from industry and sample prepared at NREL are tested extensively in our facility and compared the result.

In chapter 6, numerical result from SolTrace modeling and experimental data from on-sun testing at NREL solar furnace testing facility are compared. Limitations of test setup due to application condition are discussed with explanation.

In chapter 7, the present work is summarized and possible directions for future work are pointed out.

Chapter 2: Background

Concentrating Solar Power (CSP) Technologies are a fast-approaching renewable source for power generation. Various advanced solar thermal electricity technologies have been developed i.e. single-axis tracking, two-axis tracking, and tower technology. In single-axis tracking technology, parabolic trough collector is the established prevailing technology; however, linier Fresnel reflector technology (LFR) is heaving over parabolic trough collector technology. Dish stirling technology is a potential array two-axis tracking technology but investment costs are high [22]. Now, solar tower technology is moving to the forefront for solar to electric conversion in a large scale and with grid integration facility. This technology has the potential to reach ≤1000 ^{o}C operating temperature which allows higher power cycle efficiency than others.

Key challenges associate with solar tower technology are; receiver design to accommodate with high temperature power cycle, heliostat field for optimization of heat flux distribution on receiver's panels and heat transfer fluid that can well behave at temperature >650 ^{o}C [9, 23].

2.1 SOLID PARTICLE RECEIVER

Since 1970, solar power tower concept has been developed. In 1982 near Barstow, California, Solar One, the 10 MWe solar thermal central receiver pilot power plant first started its operation [24]. After six years' successful testing and operation, it was decommissioned in 1988. The tubular liquid central receiver operated by steam Rankine cycle with steam as the heat transfer fluid (HTF) and the cycle efficiency was only 30% [25]. Because of such a low efficiency and low heat transfer capacity of steam, the HTF was switched to molten nitrate salt (60% sodium nitrate, 40% potassium nitrate) in the Solar Two power plant. This new HTF allowed higher incident flux [26] and better heat transfer but molten nitrate salt cannot go beyond 565 ^{o}C, as it becomes unstable above that temperature. Liquid sodium [4], chloride salt [27] and fluoride-salt [28] also been

proposed as an alternative HTF to molten nitrate salt. Carbonate salts have been suggested as a HTF because of their material compatibility and affordability but at high temperature, it degrades [29]. Another concern with liquid metals or salts is it could freeze-up (usually melting temperatures are above ambient) due to equipment malfunction or operation error [30]. To alleviate this concern researcher projected to move on gaseous fluid at supercritical state like supercritical steam and supercritical Carbon-di-oxide (sCO_2). Supercritical steam and sCO_2 while operated with closed loop Brayton cycle, offers a power block efficiency ~50% compare to the conventional subcritical steam Rankine cycle efficiency of 42% [31]. In addition with addressing high temperature issue, solid particle as a HTF can be used as a thermal energy storage (TES) media so as it can store energy to supply during peak hour. This feature makes differentiating advantage to solid particle receiver (SPR) over other type of receivers. SPR is favorable than others because of low cost HTF, same HTF can be used as storage media and high efficiency due to its' direct absorption feature [9].

Solid particles in a SPR behaves like a fluidized bed. General concept is particles are dropped from the top, irradiated by direct solar incident light from the heliostat field, get heated and exit the receiver. Heated particles either exit through the heat exchanger or directly stored as a storage media in a tank. It has also been used for hydrogen production in Sandia National Laboratories; ~690 μm ceramic particle has dropped like a curtain from the top of the cavity receiver and heated up to 1000^{o}C [32]. Sandia National Laboratories in Albuquerque made a prototype SPR. They have designed a cavity type SPR where solid ceramic particles fall from the top of the tower following a curtain shape and being exposed to the sun while passing through the receiver cavity. This group did an on sun testing at Sandia's NSTTF field using sintered bauxite particles and heated the particles in excess of 900^{o}C by directly exposing to concentrated sun light [18].

Liquid based tubular receiver has been assessed extensively at Sandia National Laboratories [33, 34], Temis [35] and Platforma Solar de Almeria [36]. Two types of tubular receiver are known in power tower technology: external and cavity type receiver. Sandia designed their SPR with a cavity receiver concept but NREL's design idea is very innovative compare to the other conventional design. The design conception is very appropriate to its name "Near-blackbody solid particle receiver". The proposed design uses gas/solid, two phase flow as HTF and solid particles used as a storage medium. As intended to meet SunShot Initiative cost and performance target, this receiver is designed to use low-cost stable materials that can withstand temperatures of >1000ºC.

2.1.1 Coating Development

Modeling and physical investigation help to resolve design uncertainties related to receiver operability and ability to meet design targets. At the very initial stage I searched for literature on existing coating method and their application criteria as coating development is uncertain and time consuming. A solar plant is assumed to be operational for 25 years. So to be very affirmative on a new invention it needs to be extensively tested in lab scale before a product launch.

NBB particle receiver is designed such a way that meet the performance of the multi-zone absorber coating requirement. The front zone needs to be highly specular reflective, middle section require diffusive coating which can withstand its optical properties at >1000ºC under continuous thermal cycle and the rear section is 97% absorptive. The applied coating should maintain desired level of stability considering exposure time and temperature to satisfy the flux distribution and particle heating requirement.

Specular reflective material for flare section

Paragraphs High-specular reflectance of the entrance section of the NBB receiver design is the optical requirement for deep flux penetration inside the absorber tubes. The most common applications for this high specular reflective coating material are solar reflecting concentrators. Silver and aluminum are considered as the best solar reflectors with a reflectance value 97% and

92% respectively[37]. But the degradation rate under ambient conditions without a protection layer is rapid for both materials. Austenitic steel is a good candidate but the solar reflectance value is low (67%) [38]. Thus the optical performance of this solar reflective coating depends on their mechanical and chemical properties. Nevertheless, exposure to the environment may adversely impact the optical performance due to erosion or oxidation of the surface [39]. M. Brogren et al. introduced a new reflector material to solve this issue. Their new material system - aluminum-polymer-laminated steel reflector showed 82% of solar weighted and 77% of specular reflectance before ageing. However, after 2,000 hours in damp heat at 1,000 W/m2 heat flux, the total and specular reflectance diminished to 75% and 42% respectively and does not have long-term stability above 110°C temperature. Outdoor testing and controlled laboratory accelerated testing was performed to measure the optical performance and long-term durability in weathered conditions. Silvered thin glass mirror, silvered polymer film, and anodized sheet aluminum with a protective polymer coating was a promising candidate (80%-90% specular reflectivity) for long-term outdoor applications but none of these materials is considered for thermal cycling at high temperature. The test procedure was conducted at ambient temperature outdoors, and 60oC temperature inside a laboratory controlled environment [40, 41]. Donald A. Jaworske from NASA Lewis Research Center conducted a test at high temperature on silver as a reflective material. To avoid the oxidation of silver by oxygen, he placed the entire setup in a vacuum chamber and used silicon dioxide on top of the silver as a protective layer. His result showed that in a vacuum chamber, specular reflectivity dropped down from 91.9% to 65.1% and total reflectivity only 0.4% (from 95.1% to 94.7%) at 530oC. Kribus et al. ran a test at Weizmann solar tower facility in Israel, where they used high reflective front surface aluminum or silver reflectors in a secondary concentrator. Although they didn't map the reflectivity of the surface during testing, they reported significant reduction in reflectivity of these surfaces[42]. Broad research has been conducted on the idealized mirror reflector at ambient conditions for solar collectors or vacuum conditions for optical instrument, which has limited relevance for developing a receiver reflector that is subjected to elevated temperatures.

Relevant research has been conducted using the aforementioned reflective mirrors for high-temperature specular reflectors for the receiver applications. Fernández-García, et al, presented findings from a study on the durability and reflectivity of several reflector systems for high-temperature applications [43]. In their works, they considered two types of mirrors for use as "secondary concentrators" – 3D-CPC's for tower use above 1000 kW/m2 and 2D-CPC's for use in Linear Fresnel systems. The 3D system is water-cooled, while the 2D system is passively cooled, reaching temperatures up to 400°C. The test samples were subjected to three batches of testing including salt spray test, combined weathering testing, and high flux exposure testing where samples were exposed to flux from 590-1470 kW/m2 for 3.5 hours and 3 cycles.

MIRO-SUN® is a highly reflective material produced by Alanod, and was investigated as CPC reflector [44]. Stringent tests have been performed on Alanod MIRO-SUN® Reflector for outdoor usage. Total reflectivity in the visible range stated for outdoor use is 90.6% reported in the Alanod brochure and measured by the NREL Optical Material Lab.

While the silver-glass mirror and Alanod reflector has several positive attributes as described above, the material can only be applied in the planar form. They are difficult to be applied for the water-jacket design developed due to the hexagonal flared tube-entrance section. There are additional quality concerns such as the formation of voids inside the adhesion layer to the substrate. The adhesion method for glass mirror and Alanod needs to be developed and verified.

Unprotected silver surfaces readily oxidize in air, especially at elevated temperatures. To guard against silver oxidation, a protective, transparent top coating must be applied to the reflective silver coating. CVD deposited thin films of silica have been used to protect front surface silver mirrors with some success and recent developments in silica sol-gel technology have led to the development of sol-gel methods that produce thin films of silica (<200 nm) to be successfully applied as coatings to protect against oxidation of metals at elevated temperatures [45] and maintain optical reflectance [46]. In addition, sol-gel dip-coating methods are practical alternatives to conventional CVD processes, especially for coating large, complex geometries of receiver absorber panels.

For practical reflective surface formation, an alternative option is to use Ag coating and then coating it with a transparent thin film to provide a barrier to oxygen and limit the coating degradation. This type of reflective coating has a specular solar reflectivity of 95% and showed no degradation in reflectivity after 72 hours in a conventional oven at 300˚C [47, 48]. A sol-gel method to protect silver mirror coatings is being tested to verify another protective method [48]. The protected Ag-mirror coating consisting of electrodeposited silver with a thin film of silicon dioxide applied by a sol-gel method was tried as front covered mirror. Sol-gel is a chemical synthesis technique in which an oxide network forms in a liquid through hydrolysis and condensation reactions. The "sol" is a liquid in which colloidal particles or polymers disperse in a solvent. The "gel" is a solid like three dimensional interconnected nanostructure network, which encloses a liquid phase. This technique has been widely used in glass and ceramics manufacturing industry [49]. But more recent applications of the sol-gel technique include electrical, optical [50, 51], medical science [52, 53], protection coatings [54, 55] and solar energy applications [56]. For the past several years, sol-gel technology has been tried in solar energy applications. C.J. Brinker in collaboration with Sandia National Laboratories first applied this technology as antireflection coatings of SiO_2 and TiO_2 on silicon solar cells and protective coatings applied on top of silvered stainless substrate [56]. They reported in their aging test, the average specular reflectance of silver-plated stainless steel coated with sol-gel thin film was 0.90-0.91.

Based on the literature review, several reflective coating methods were screened for potential use in the NBB receiver design: Generally, the coating should be cooled below 200°C for most of the reflective materials. More details on sample screening, sol-gel preparation and lab-scale testing will be found in chapter 5.

Chapter 3: Numerical Analysis

The reliability of the numerical analysis approach is a matter of big concern to engineers and scientists. It is limited by the computational resources, the accuracy of numerical models, proper boundary conditions etc. With the invention of affordable high performance parallel computers and advances in computational techniques in recent years, it is able to deal with and study real life problems with significantly better accuracy.

Numerical analysis is subjected in this work to evaluate the design and performance testing of the near black body solid particle receiver. Computational Fluid Dynamics (CFD) modeling software ANSYS 14.0 was employed to check out the granular flow patterns of the solid particle around the hexagonal tube array for different configurations and inclination angles and the heat flux distribution with appropriate radiation model. Chemical Reaction and Equilibrium software HSC 7.0 was run to predict coating material stability profile during thermal cycling. NREL's SolTrace beam characterization software were used for mapping the heat flux on prototype receiver design for on-sun testing condition based on Sandia's NSTTF field and the solar furnace testing for a single tube empirical design.

3.1 Governing Equations for Fluid Flow and Radiation Modeling

The fluid flow pattern around the hexagonal tube array is an Eulerian-Eulerian or two-fluid model (TFM) computational problem. Eulerian-Eulerian approach is not suitable for tracking individual solid particles like DEM, rather it suits for a control volume. Here both fluid and solid phases behave like interpenetrating continuua with each other. This inter-phase exchange for each phase is solved by continuity and momentum equations. Equation 4.1 is the continuity equation where i denote for either fluid (f) or solid (s) phase.

$$\frac{\partial}{\partial t}(\alpha_i \rho_i) + \nabla.(\alpha_i \rho_i \overrightarrow{v_i}) = 0 \tag{1}$$

Equations 3.2 and 3.3 are representing the momentum equations for both the solid and fluid phases

$$\frac{\partial}{\partial t}(\alpha_s \rho_s \overrightarrow{v_s}) + \nabla.(\alpha_s \rho_s \overrightarrow{v_s}\overrightarrow{v_s}) = -\alpha_s \nabla p - \nabla p_s + \nabla.\overrightarrow{\tau_s} + \alpha_s \rho_s \vec{g} + K_{sf}(\overrightarrow{v_f} - \overrightarrow{v_s}) \tag{2}$$

$$\frac{\partial}{\partial t}(\alpha_f \rho_f \overrightarrow{v_f}) + \nabla.(\alpha_f \rho_f \overrightarrow{v_f}\overrightarrow{v_f}) = -\alpha_f \nabla p + \nabla.\overrightarrow{\tau_f} + \alpha_f \rho_f \vec{g} + K_{sf}(\overrightarrow{v_s} - \overrightarrow{v_f}) \tag{3}$$

Neglecting the viscous dissipation, the energy equation for fluid and solid phases become

$$\frac{\partial}{\partial t}(\alpha_i \rho_i H_i) + \nabla.(\alpha_i \rho_i \overrightarrow{v_i} H_i) = \nabla.\alpha_i K_{i,eff} \nabla T_i - h_{if}(T_i - T_j) \tag{4}$$

Surface-to-surface radiation model is considered when radiative heat transfer occurs between the granular particles and the tubes surface. FLUENT calculates the value of radiosity *J* and this value are then used to calculate the wall temperature of the faces in the cluster. The heat flux distribution is constant on each faces so the average temperature value of the surface cluster would not be impacted much by the highly non-linear radiation source term (proportional to the fourth power of temperature). Following equation is used to calculate the average surface cluster temperature [57].

$$T_{SC} = \left(\frac{\sum_f A_f T_f^4}{\sum A_f}\right)^{1/4} \tag{5}$$

Here, T_{SC} is surface cluster temperature, A_f is the area of face f and T_f is the temperature of face f. Summation determines the average temperature.

3.2 HSC CHEMISTRY

HSC chemistry has a wide range of applications in scientific research and industry. It is also a useful tool in educational sector for chemical practical and studies. The objective of using

this software is to make fast and easy thermodynamic calculations of chemical reactions. It is facilitates with different calculation methods which offers the knowledge of different variables' effects in an equilibrium system. The Eh-pH diagrams present the corrosion and dissolution behavior of materials and thermodynamic stability areas of compositions in a chemical reaction. Thermodynamic stability is presented as a function of pH and electrochemical potential scales.

Here in this thesis work, HSC Chemistry modeling was used to predict the chemical thermodynamic stability of elctroless metal coating at the temperature range of 0-1000ºC. For prediction it uses the thermodynamic data from its large database [58]. Numerical analysis results the change in Gibbs Free Energy. ΔG in equilibrium condition, but it does not provide any information about the reaction kinetics of non-equilibrium compositions. Equilibrium calculations show the impact of product composition for temperature variables and raw materials quantity. It also tells about the amount of prevailing phases in a reaction.

3.3 SOLTRACE MODELING

This is optical analyzing software developed at the National Renewable Energy laboratory (NREL) [59]. It has been used for performance analysis of solar power optical system in CSP power plant. This ray tracing tool models the heliostat field to map the heat flux distribution on high temperature receiver. Accuracy of the result depends on the number of rays to be traced. Larger number of sun rays will give more accurate result but will consume more processing time and computationally expensive. It can resemble the heliostat field according to desired power output for a defined geographic location. It is very handy software for scientific research in CSP applications.

Three right-handed coordinate systems have been used in SolTrace for optical characterization: the global coordinate system, the stage coordinate system and the element

coordinate system. In a stage coordinate system, each element is defined according to its location and orientation i.e. local coordinate system. However, each stage coordinate system is defined associating with its global coordinate system. Sun location is also specified based on the global coordinate system. Input of sun direction can be either in vector format or in time format with specified latitude. Figure 3.2 illustrates this phenomenon [60].

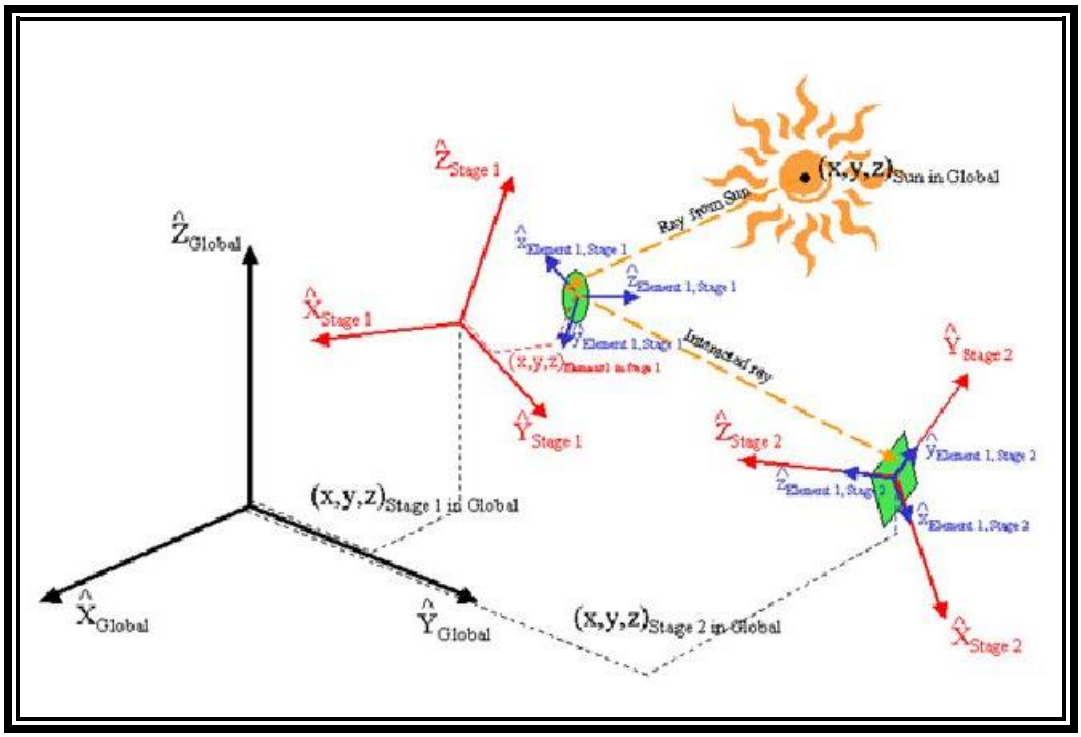

Figure 3.1: Coordinate systems in SolTrace

The purpose of using SolTrace modeling software is to predict the solar flux map on the high temperature receiver tubes which may help to guide the prototype design for fabrication and performance validation. It also envisions the reflective coating performance inside the tube wall through the flux mapping. A Fortran script compatible with SolTrace, helps the flux map readable for Fluent simulation software. Therefore the flux map input in Fluent can be comparable to real heliostat field instead of assuming constant heat flux throughout the tube. This boundary condition advantages to have more accurate result.

Chapter 4: Methodology

This chapter content includes the design module of the near black body (NBB) high temperature receiver and the approach of coating application on the hexagonal tube array. Discussion also continues on the hemispherical and specular reflectivity measurement procedure and how to attain a specular reflectivity <70% at flare section of the tube, which is the insistent part of this thesis work.

4.1 Geometry of the Near Black Body Solid Particle Receiver

The performance of granular particles as a heat transfer fluid is more satisfactory compare to the conventional liquid heat transfer fluid in CSP power plants. These solid particles eliminate the issue of thermal stability at higher temperature and it could easily deal with ≤1000^{o}C operating temperature. Like the liquid HTF, it doesn't have fluid freezing risk. Moreover, the thermal to electric conversion efficiency is very high with this fluidized bed NBB solid particle receiver.

The design and fabrication of a solid particle receiver with ≤90% efficiency, is a challenge. This NBB enclosed particle receiver design intends to resolve the issues found in other types of particle receiver such as German DLR fixed and centrifugal falling particle receiver and Sandia's open-cavity falling particle receiver [18, 61, 62]. It facilitates with enough residence time to reach at 1000^{o}C temperature while being exposed to concentrated solar flux, within a single pass. Thus it does not require additional particle-lifting parasitic power consumption, which also reduces cyclic thermal losses.

The concept of the NBB enclosed solid particle receiver is the use of a tubular absorber to collect heat flux from the heliostat field and heat up the granular particles while passing through the channel between the hexagonal tube array. Figure 4.1 is the detailed single tube geometry of NBB enclosed solid particle receiver. The flare section of the tube will have high specular

reflective inner surface which will help spreading the flux inside the tube. The inner tube surface will have diffuse reflective surface ≤70% for uniform heat flux distribution throughout the tube. This flux spreading will help to achieve desired high temperature on the tube wall surface so that the granular solid particles get enough heat from the tube wall to reach 1000^{o}C temperature.

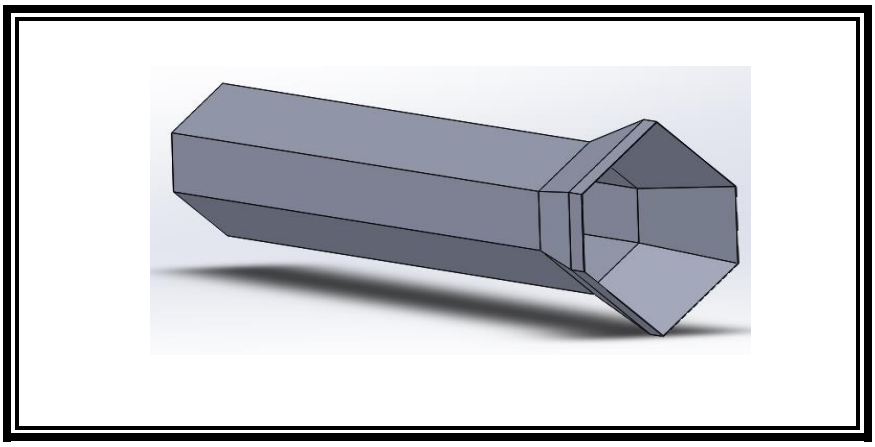

Figure 4.1: Single hexagonal tube geometry of NBB enclosed solid particle receiver.

Multiple array of hexagonal tubes will be arranged like figure 4.2, in a prototype receiver. Every single tube will be laser welded on the flare section with a water jacket so the flare section temperature can be maintained at 150^{o}C. Solid particles will flow through the inter-tube space and collect heat from tube wall surface.

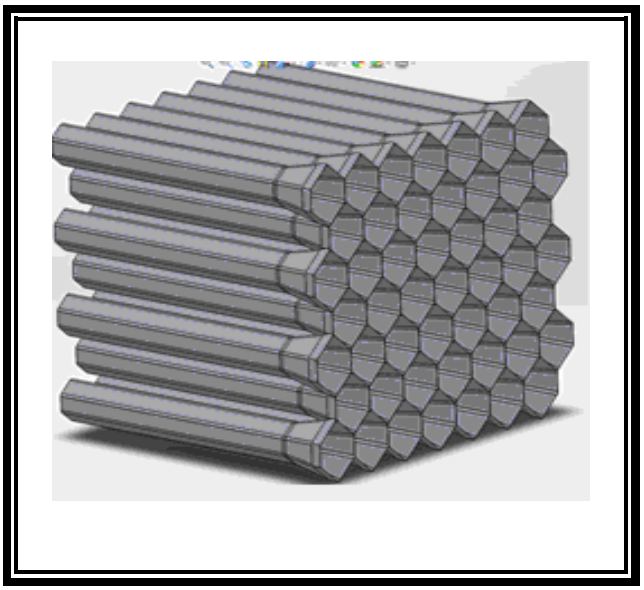

Figure 4.2: Multiple hexagonal tube arrays in NBB enclosed solid particle receiver

4.2 INTRODUCTION OF COATING

In general, coating is defined as a process that applied on top of a substrate which forms a film to impart corrosion resistance to the surface. Here the purpose is to find an absorptive coating and corresponding application methods that can be used to coat the flux-adsorbing surface (inner surface) of receiver tubes and create near-uniform flux adsorption and temperature distribution within the receiver tubes. To prolong the uniform flux distribution towards the enclosed end of the receiver tubes, the applied coating should have appropriate level of specular reflectance. Receiver tubes geometry enquires higher reflectance at the tube aperture and fading the specular reflectance towards the enclosed tube end. The specific axial and angular dependence of reflectance depends on the receiver tube geometry and the incident flux distribution. Appropriate coatings need to be thermally stable in air at temperatures up to 1000ºC and must tolerate thermal cycling on a daily basis through the entire project life. Promising coatings need to be applied economically to an array of receiver tubes (inside the tubes) with complex geometry to generate a receiver panel that possesses the desired optical properties.

For solid particle receiver tubes design, the preferred approach to have uniform flux distribution is to incorporate the coating along the axial length of the receiver tubes. Necessities of uniform flux distribution across the tube area are: 1) maximize the heat transfer between solid particle flow and tube surface area, 2) meet the average target particle exit temperature 800^{o}C, 3) eliminate temperature cloud on the tubes surface, and 4) minimize receiver's heat loss. A solar receiver with these properties is critical to the optimal performance and lifetime of the power tower plant. It is crucial to identify the best match coating material and the application of coating on top of the metal surface at that high temperature for a number of thermal cycles. So a test protocol was developed to determine if the optical properties of the coating(s) will withstand high temperatures and temperature cycling that is representative of an operating solar receiver.

4.3 TYPES OF COATING

Several techniques are available for depositing metal and metal oxide coatings, however, only a few techniques are practical and economical for coating large, complex surfaces. Another important factor was considered while choosing the coating material and approach that it should have specular reflectance properties >70% at >200^{o}C for flare section and >1000^{o}C for middle section those can sustain thermal cycling at specified temperature. With consideration of these criteria, three types of technique for several types of material substrate samples were included in the test protocol, i.e. 1) Electroplating, and 2) Thermal spray or Plasma spray 3) Aerosol spray.

4.2.1 Electroplating

In this process metal coatings are applied on top of a solid metal substrate by electro-chemical deposition. Transition metals or anodes are deposited as a layer of coating onto a solid

substrate while electrical current flows through the aqueous solution. Current flow oxidized the metal atoms of anode and makes the metal ions to be deposited onto the cathode surface (solid substrate). Transition metal includes nickel, chromium, copper and their alloys. Gold can also be deposited using electroplating techniques but gold ion (Au+1) is only stable in aqueous solution when it bonds with cyanide ion (CN-1) to form Au (CN)2-1.

Electroplating is applicable for both uniform and non-uniform geometry. For this high temperature receiver tube module, electroplating might be a considerable technique to apply metal/metal alloy coatings inside the receiver's tube. In this method it is possible to create a thickness gradient along the axial tube direction that makes electroplating spectacular from other coating application methods. This thickness gradient is account for reflectance variance from the aperture to the enclosed end of the receiver's tube.

Electroplating coating proceeding

For this high temperature receiver design it is very crucial to have high specular reflectance on the aperture of the tube. So the objective is to identify a specular coating which can well behave at desired high temperature (>200^{o}C) for number of thermal cycles over 30 year life time. To do so a coating test plan was followed particularly for electroplating methods.

A commercial partner prepared the sample material of 310 Stainless Steel (SS) coupon with dimension $1''X\ 1''\ X\ 0.060''$, one side polished. 5 different coating materials applied on the 310 SS substrate and prepared 41 coupons to identify the specific coating configuration from these options. Selected materials are:

- C_{none}: no coating (SS 310 polished)
- C_{Ni}: Electroless nickel plating
- $C_{Ag/Ni}$: silver coated on nickel
- $C_{Au/Ni}$: gold coated on nickel
- $C_{Au/Ag/Ni}$: gold and silver coated on nickel

These coating materials were applied with different thickness to determine the thickness gradient effect on specular reflectance and the coating behavior at high temperature. Table 4.1 is showing the coating configuration with different thickness.

Table 4.1: Coating materials and thickness configurations

Thickness (mil=1e-3 inch)		Coating –Au on Ni			Au above Ag on Ni		Note
		Ua*	Ub	Uc	Ga*	Gb	
Ni	Thickness	1.0	0.5	1.0	0.5	1.0	• Electroless Ni plating. • Leave 3 pieces of 1mil Ni coating without noble metal coating
	Pieces (total 38)	8	5	7	6	12	

Ag	Thickness	-	-	-		0.5	1.0	Leave 2 pieces of 1.0 mil Ag coting without gold coating
	Pieces					6	12	
Au (/Ni)	Thickness	0.25	0.25	0.5		0.25	0.25	Gold is typically mixed with nickel for the coating #Leave 3 pieces of Gb with pure Au coating;
	Pieces	5	5	4	3#	6	10	

The acronyms (Ua, Ub, Uc, Ga and Gb) stand for a configuration of coating material thickness. For example, Ga means an Au layer with thickness of 0.25 mil, an Ag layer with thickness of 0.5 mil and a Ni layer with thickness of 0.5 mil.

** 1 mil = 1e-3 inch.

The coated samples are numbered for tracking. 41 samples are categorized into 9 (Table 3.2) different groups considering its thickness and reflective properties.

Table 4.2: Coating sample summary

Sample Number	Coating method	Reserve	(1 mil Ni)	(1mil Ag; 1 mil Ni)	Ua	Ub	Uc	Ga	Gb
3	C_{none}	3 (N1~N3)	-	-	-	-	-	-	-
3	C_{Ni}	-	3 (N4~N6)	-	-	-	-	-	-
2	$C_{Ag/Ni}$	-	-	2 (N7~N8)	-	-	-	-	-
14	$C_{Au/Ni}$	-	-	-	5 (N9~ N13)	5 (N14~ 18)	4 (N19~ N22)	-	-
3	$C_{Au^{\#}/Ni}$	-	-	-	-	-	3 (N23~25)	-	
16	$C_{Au/Ag/Ni}$	-	-	-	-	-	-	6 (N26~ N31)	10 (N32~ 41)

After having the samples ready, those were prepared for measuring hemispherical and specular reflectance with respect to acceptance angle, incidence angle and wavelength under different thermal condition. For better accuracy, all the samples are prepared commercially. Before sending to the oven, all samples surface cleaned with acetone and then dried with nitrogen gas shooting from a gun at certain pressure. Section 4.3.1 has a detail discussion about reflectance measuring instrument.

4.2.2 Thermal Spray Coating

Thermal spray coating is a well-established coating process to apply metallic or non-metallic coating onto a substrate. In this method, an energy source is used to heat the coating material (in the form of powder, rod or wire) that propelled the hot particles to the cold substrate with high velocity. A nickel bond coat has been used in between the ss310 substrate and the aluminum oxide coating layer. The sample doesn't need any further curing process as the coating layer applied on the surface at high temperature. Based on the application, thermal spray can be distinguished into three major categories: flame spray, electric arc spray and plasma spray [63]. In this method, an energy source is used to heat the coating material (in the form of powder, rod or wire) that propelled the hot particles to the cold substrate with high velocity (Figure 4.3).

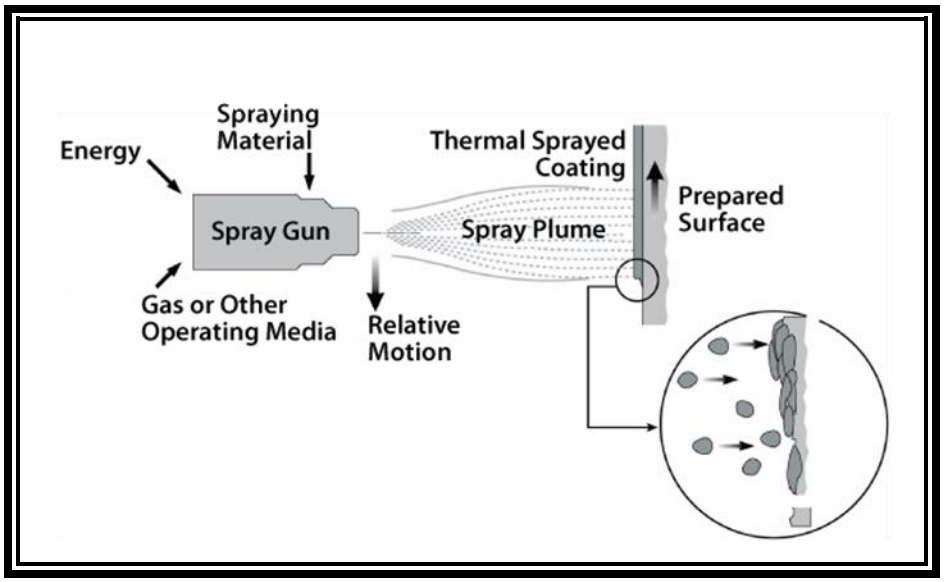

Figure 4.3: Thermal spray coating [64]

To meet the prerequisite of 70% specular reflective surface coating for high temperature receiver tube, thermal spray ceramic coating was applied onto 310 SS substrate in combination with a bond coating. The coating application has been done in Sandia National Laboratories at their Thermal Spray lab with the help of their expertise. They have used a bond layer in between Al_2O_3 (alumina) and the stainless steel substrate. The fine finished sample was then tested for thermal cycling at 800^{o}C. Detail discussion will be found in result and discussion chapter.

4.2.3 Aerosol Spray Coating

Aerosol spray is commercially available refractory paint. The reason to look over this spray is to compare the reflectivity of ceramic paint applied by thermal spray coating method. Three different types of refractory paint have been considered for performance test which are easily available in the market. This paint has been used on the substrate without bond coating and applied directly onto the substrate. The curing process was followed according to the instruction for each type of refractory paint. Al_2O_3 and ZrO_2 were cured for 30 minutes at 600^{o}C temperature and silica based ceramic paint were cured for 1 hour at 600^{o}C temperature. Before applying the paint, the

substrate surface was coarsen with abrasive paper and then cleaned. This rough surface helps to hold the aerosol spray more rigidly. All of the paints have easy application and can sustain at very high temperature range. Automotive industry has more frequent use of this coating specifically in exhaust pipe. It has good thermal, molten salt, acid, alkali and oxidation resistance.

Polishing

Polishing on a metal surface enhance the specular reflectivity of substrate's surface. The abrasive particles of the polishing agent give a smooth and glossy finishing over the surface. The polishing compounds make the abrasive particles uniformly dispersed throughout the surface and maintain a uniform viscous surface [65]. The application process is either directly by hand using a soft fabric on the coating surface or polish the substrate surface using appropriate abrasive cloth/paper in a polishing machine.

Mirror polish is a must criteria to get better specular reflective surface i.e. specular reflectivity increases by a percent if the substrate is mirror polished before electroplating/coating [66]. More details explanation will be found in section 4.3.1.

4.3 METHODOLOGY FOR CHARACTERIZING THE REFLECTANCE OF COATING SAMPLES

Along with excellent specular reflective properties (<70%), the applied coating should have the feasibility to withstand 800^{o}C for a particular time of exposure daily considering 30 years plant life cycle. This feature is significant for receiver's thermal efficiency as well as overall plant efficiency.

4.3.1 Reflectance

Reflectance ρ of a surface is a function of incident light wavelength λ, incidence angle θ and the size of reflecting light acceptance surface $S(\Omega)$ [67].

$$\rho = \rho(\lambda, \theta, S(\Omega)) \tag{4.1}$$

Here, Ω is the solid angle of the reflecting light acceptance surface S, unit steradian. Reflectance can be classified in two ways based on acceptance surface S, i.e. hemispherical reflectance and specular reflectance. Hemispherical reflectance is considered for wide range solid angle ($\Omega = 2\pi$), whereas specular reflectance counts only for small aperture acceptance angle, φ.

$$\rho_{Spec}(\lambda, \theta, \varphi) = \frac{\int_0^{\Omega(\varphi)} g_{Spec}(\lambda,\theta,\varphi).d\Omega}{E_{in}} \tag{4.2}$$

In solar field, specular reflectance has high-powered impact on receiver's efficiency. High temperature receiver can only capture the reflected rays from heliostat field if it's within an angular cone on the order of ten miliradian (mrad) [68-70]. When the incoming light hits the mirror surface and reflected towards specular direction with aperture acceptance angle, φ, is called specular reflectance (Figure 4.4).

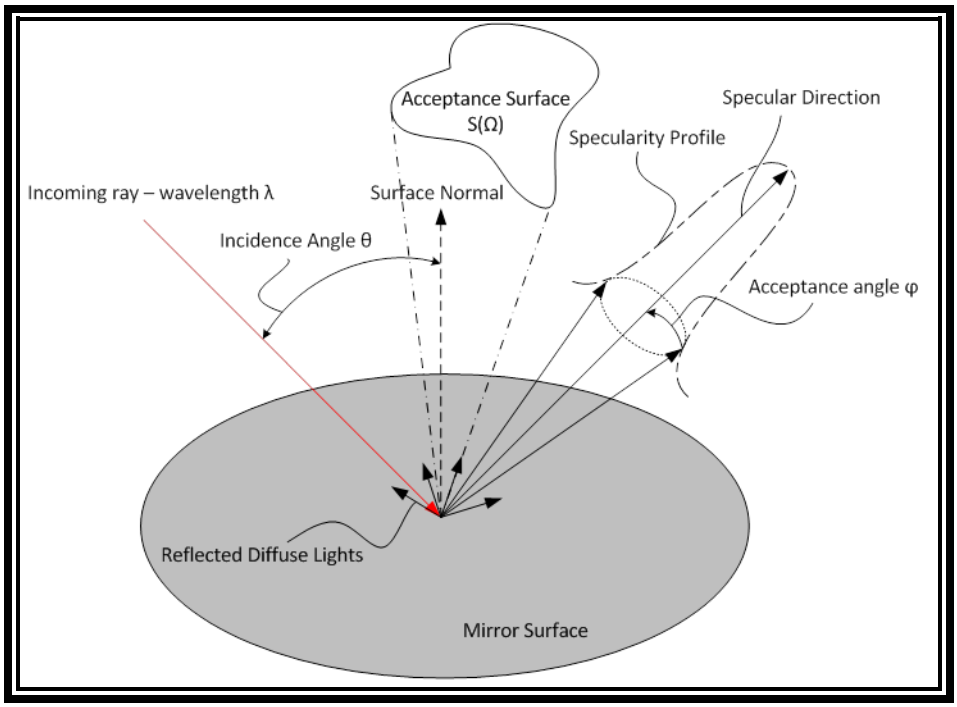

Figure 4.4: Mirror reflectance for an incident light [67]

Two optical features; specular reflectance and specularity are the determinant of a specular surface. Like the specular reflectance, specularity is also a function of incidence light wavelength, incidence and acceptance angle. Not all the incident light bounce back towards the specular direction, some of them are diffused because of the microscopic texture irregularity of the mirror surface. So, the mirror reflectance is a combination of specular and diffuse reflectance.

$$\rho = \frac{\int_{S(\Omega)}[g_{diff}(\lambda,\theta,\varphi)+g_{Spec}(\lambda,\theta,\varphi)].d\Omega}{E_{in}} \quad (4.3)$$

Here E_{in} is the incident radiating energy that hits the surface.

In heliostat field, sun rays hit the mirror surface and then the solar spectrum spans about 280 nm to 2,500 nm [71]. It follows a specific power intensity distribution as a function of light wavelength. Therefore most CSP applications affirm with solar weighted values on specular properties. The solar collector is exposed to the concentrated sun light during operational hours at

high temperature. So, the specular properties of the coated receiver's surface might be temperature dependent.

The mathematical model of specular reflection, namely, solar weighted specular reflectance $\rho_{spec}^{SW}(\varphi)$ and mirror specularity $f^{SW}(\varphi)$, is then defined as follows:

$$\rho_{spec}^{SW} = \rho_{spec,tot}^{SW} \int_0^{\Omega(\varphi)} f^{SW}(\varphi) \cdot d\Omega \tag{6}$$

Here, the solar weighted total specular reflectance is:

$$\rho_{spec,tot}^{SW} = \frac{\int_0^{\infty} \int_0^{\pi/2} E(\lambda) \cdot F(\theta) \cdot \rho(\lambda, \theta, \pi) \cdot d\lambda d\theta}{\int_0^{\infty} \int_0^{\pi/2} E(\lambda) \cdot F(\theta) \cdot d\lambda d\theta} \tag{7}$$

Here, $E(\lambda)$ is the direct normal irradiance spectrum as a function of light wavelength [72] and the majority of solar power lies in a light wavelength range of 280 nm to 2500 nm[71, 73] $F(\theta)$ is a weighting function for the incidence angle θ, which typically depends on the specific solar application but is often approximated as a Dirac delta function centered at a representative incidence angle of this solar application. Similarly, $f^{SW}(\varphi)$ is the normalized form, weighted over the light wavelength λ and incidence angle θ:

$$\int_0^{\infty} f^{SW}(\varphi) \cdot d\Omega \cong \int_0^{2\pi} \int_0^{\varphi_{spec}} f^{SW}(\varphi) \cdot \sin(\varphi) d\varphi d\beta \cong 1 \tag{8}$$

Here, the spherical coordinate system used refers to the specular direction as the zenith and β is the azimuth angle [67].

4.3.2 Reflectivity Measuring Instrument

Hemispherical reflectance are measured for wide range of light wavelength for a large incidence angle whereas, specular reflectance are measured for small aperture acceptance angle for a small bandwidth. The optical material lab in National Renewable Energy Laboratories facilitates with a wide range of instrument to measure the mirror surface reflectivity and reflectance property. These instruments used to measure various types of reflectance with respect to acceptance angle, light wavelength and incidence angle under varying reflector conditions. In

particular, SOC – 100 HDR is the only instrument able to measure reflective/absorptive properties of coating surface under high temperature up to 500 °C. For the scope of work here, D&S and SOC-410 Solar reflectometer are selected to characterize the optical performance of the coating samples.

Table 4.3: List of reflectance measuring instrument

Name of Instrument	Capability	Measurement conditions
D&S-1 (1)	Specular at 660 nm: • 7 mrad • 15 mrad • 25 mrad	ambient, portable
D&S-2	Specular at 660 nm: • 7 mrad • 25 mrad • 46 mrad	ambient, portable
SOC-410 Solar [74]	solar weighted reflectance: • total specular reflectance; • hemispherical reflectance; • diffuse reflectance	ambient, portable
SOC – 100 HDR [75]	Hemispherical, specular reflectance as a function of incidence angle and light wavelength in the IR range.	Under high temperature up to 500°C

Measurements by each type of reflectometer are denoted as below to facilitate the data post-processing:

Measurement by D&S-1 and D&S-2 are denoted as;

$$\rho_{spc}^{660,m}(\varphi_i), i = 1,2,3,4. \tag{9}$$

Here, m is the number of metallic coating sample and

$$\varphi_1 = 3.5\,mrad; \quad \varphi_2 = 7.5\,mrad; \quad \varphi_3 = 12.5\,mrad; \quad \varphi_4 = 23\,mrad; \tag{10}$$

All the measurements for D&S are conducted for 660 nm wavelength

Measurement taken by SOC-410 are denoted as

$$\rho_{spc,tot}^{SW,m} \tag{11}$$

This measurement is taken for solar weighted total specular reflectance of the coating surface.

Instrument SOC410 has been used for both hemispherical and specular reflectivity measurement, though the specular reflectivity value it gives for 105 mrad (mili radian) acceptance angle. At first the instrument was calibrated using a diffuse coupon, a mirror coupon and a black body pipe; and then the sample coupon was placed on top of the incoming light for measurement. The data analysis showed the reflectivity measurement as a function of wavelength. Instrument D&S 1 and D&S 2 were used for surface specular reflectivity measurement. D&S 1 gives reading for 7, 15 & 25 mrad acceptance angle, whereas D&S 2 is able to measure at 7, 25 & 46 mrad acceptance angles.

Chapter 5: Sol-Gel Coating

This chapter content discuss about a thin film formation on top of a reflective surface which is called Sol-gel thin film formation. Discussion also report past work progress, current development and extensive lab-scale test result.

5.1 Introduction To Sol-gel Coating

Silver and aluminum are considered as the best solar reflectors with a reflectance value 97% and 92% respectively [37]. But unprotected silver surfaces tend to degrade in ambient air, especially at elevated temperatures. For practical reflective surface formation, a protective, transparent top coating can be applied to provide a barrier to oxygen and to limit the coating degradation.

CVD (Chemical Vapor Deposition) deposited thin films of silica have been used to protect front surface silver mirrors with some success, and the developments in silica sol-gel technology have led to the development of sol-gel methods that produce thin films of silica (<200 nm) to be successfully applied as coatings to protect against oxidation of metals at elevated temperatures and maintain optical reflectance [76]. Sol-gel is a chemical synthesis technique in which an oxide network forms in a liquid through hydrolysis and condensation reactions. The “sol” is a liquid in which colloidal particles or polymers disperse in a solvent. The “gel” is a solid like three dimensional interconnected nanostructure network, which encloses a liquid phase. This technique has been widely used in glass and ceramics manufacturing industry [49]. More recent applications of the sol-gel technique include electrical, optical [50, 51], medical science [52, 53], protection coatings [54, 55] and solar energy applications [56]. Sol-gel dip-coating methods are practical alternatives to conventional CVD processes, especially for coating complex geometries of heat shield with hexagonal openings.

Silver coating with a sol-gel protective coating has a specular solar reflectivity of ~95% and past studies have shown no degradation in reflectivity after 72 hours in a conventional oven at

300°C [76]. The sol-gel method to protect silver mirror coatings has been tested to verify the protective method. The protected mirror coating consisting of electrodeposited silver with a thin film of silicon dioxide applied by a sol-gel method was tried as front covered mirror [76]. Brinker in collaboration with Sandia National Laboratories first applied this technology as antireflection coatings of SiO_2 and TiO_2 on silicon solar cells and protective coatings applied on top of silvered stainless substrate [56]. They reported in their aging test, the average specular reflectance of silver-plated stainless steel coated with sol-gel thin film was 0.90-0.91.

NASA Lewis Research Center conducted a test at high temperature on silver as a reflective material. To avoid the oxidation of silver by oxygen, he placed the entire setup in a vacuum chamber and applied silica on top of the silver as a protective layer. His result showed that in a vacuum chamber, specular reflectivity dropped down from 91.9% to 65.1% and total reflectivity only 0.4% (from 95.1% to 94.7%) at 530oC. Kribus et al. ran a test at Weizmann solar tower facility in Israel, where they used high reflective front surface aluminum or silver reflectors as a secondary concentrator. Although they didn't map the reflectivity of the surface during testing, they reported significant reduction in reflectivity of these surfaces [42]. The literature review on high-temperature mirror reflector indicates that it is very difficult to obtain a mirror reflective surface working at high temperatures of above 400°C.

More recently, Fernández-García, et al. presented findings from a study on the durability and reflectivity of several reflector systems for high-temperature applications [77]. In their work, they considered two types of mirrors for use as secondary concentrators — 3D-CPC's for tower use above 1,000 kW/m2 and 2D-CPC's for use in Linear Fresnel systems. The 3D system was water-cooled and the mirror for the 3D system was tested to 85°C, while the 2D system was passively cooled, reaching temperatures up to 350°C. The test samples were subjected to three batches of testing including salt spray testing, combined weathering testing, and high flux exposure testing where samples were exposed to flux from 590-1470 kW/m2 for 3.5 hours and 3 cycles.

5.2 SOL-GEL PROTECTIVE-COATING METHOD

Sol-gel synthesis is used to produce an interconnected 3-D network with well-defined shapes and structures. This process mostly uses liquid alkoxide as a precursor, such as Si(OR)4, where R is an alkyl group (CxH2X+1). In a silica sol-gel process, precursor tetraethyl orthosilicate Si(OC2H5)4 is hydrolyzed by mixing with water in a certain ratio [78, 79].

$$\equiv \mathrm{Si} - \mathrm{OR} + \mathrm{HOH} \xrightarrow{\text{hydrolysis}} \equiv \mathrm{Si} - \mathrm{OH} + \mathrm{ROH}$$

In the above hydrolysis reaction, alkoxide groups $(-\mathrm{OR})$ are replaced with hydroxyl groups $(-\mathrm{OH})$ and forming alcohol molecules (ROH). Water concentration affects the kinetics of hydrolysis, i.e. small amount of water tends to slow down the hydrolysis because of light reactant concentration, while a large amount of water concentration shows same tendency due to reactant dilution [79].

In the two step condensation process, hydrated silica reacts with the released alkoxide groups $(-\mathrm{OR})$ and form $\equiv \mathrm{Si} - \mathrm{O} - \mathrm{Si} \equiv$ bonds. By-products of this reaction are water and alcohol.

$$\equiv \mathrm{Si} - \mathrm{OH} + \equiv \mathrm{Si} - \mathrm{OR} \xrightarrow{\text{alcohol condensation}} \equiv \mathrm{Si} - \mathrm{O} - \mathrm{Si} \equiv + \mathrm{ROH}$$

$$\equiv \mathrm{Si} - \mathrm{OH} + \equiv \mathrm{Si} - \mathrm{OH} \xrightarrow{\text{Water condensation}} \equiv \mathrm{Si} - \mathrm{O} - \mathrm{Si} \equiv + \mathrm{H_2O}$$

Here, alcohol is used as a solvent to blend alkoxide and water thus facilitating the hydrolysis process [80]. Inorganic polymerization proceeds in the condensation process, hence SiO_2 nanoparticles form. These particles then agglomerate and form a network by linking. The network expands all through the liquid medium, controls the thickening (i.e. density) of the medium and forms gel. This porous structure is influenced by the R ratio $(\mathrm{R} = [\mathrm{H_2O}]/[\mathrm{Si(OR)_4}])$ and the pH value. Generally, acidic solutions produce a compact micro-porous structure on the order of <2 nm [78, 79, 81].

5.3 INFLUENCE OF PARAMETERS

Sol-gel process is influenced by numerous parameters, but most dominants parameters are precursor and solvent, pH value of the solution, TEOS:H_2O molar ratio and sintering temperature.

After sintering, the final deposited SiO_2 layer film thickness depends on dipping speed. Table 5.1 describes discrete phenomenon happened by dominant parameters in sol-gel process.

Table 5.1: Influential parameters of Sol-Gel coating

Precursor	Alkoxide e.g. TEOS [$Si(OCH3)_4$], TMOS [$Si(OC2H5)_4$]	Affects the rates of hydrolysis and condensation reaction, high TEOS concentration increase solution's viscosity
pH	<pH 2, pH 2-7, >pH 7	Acidic solution has higher viscosity than neutral or base-catalyzed solution
TEOS:H2O molar ratio	R denotes the molar ratio	At R=2, incomplete hydrolysis; increasing of R value decreases organic particles from the solution
Sintering temperature	Temperature ranges from 100-500^oC	Affects porosity of the network and pore size of the particles
Dipping speed	Dipping speed varies from 5-200 mm/min	Film thickness, surface smoothness and optical performance as a protective layer

Precursor: Commonly used alkoxides used in sol-gel process are, tetraethyl orthosilicate (TEOS) or tetra methyl orthosilicate (TMOS). Advantages of using silicon alkoxide are it's transparency, physical and chemical stability, slow in reaction rate with water without catalyst and good mechanical strength. These alkoxides are prepared by adding alcohol with silicon tetrachloride (SiCl4) [82]. This reaction maintains a good homogeneity.

$$SiCl_4 + EtOH \rightarrow Si(OEt)_4 + 4HCl$$

Aelion et al. [83] and Hench [84] showed in experiment that TEOS has the primary effect on reaction rate constant and alcohol has the secondary effect. Reaction rate accelerates with types of alcohol and the increased amount of TEOS in acidic solution [85]. As a precursor, increase in TEOS concentration also increases the viscosity of the solution. But it does not have any impact on solution's density or particle size [86]. Moreover, an increased EtOH:TEOS molar ratio decrease the pore size of the network [87].

pH/Catalysts: In sol-gel process pH value of the solution play a dominant role on both hydrolysis and condensation reaction. Usually reaction rate of silicon alkoxide with water is very low. Therefore acid or base is used as a catalyst to accelerate the reaction process; e.g. addition of HCl as a catalyst can reduce the gelation of TEOS from 1000 hrs to 92 hours [82, 88]. Moreover catalyst has an impact on the pore size of the network structure and the density of the solution. Acidic solution can obtain a fine, dense network than base solution [85, 86, 89].

TEOS:H_2O molar ratio: The hydrolysis and condensation kinetics are mainly influenced by the TEOS to H2O molar ratio, which is denoted by R. If R value is too low (R=2), hydrolysis reaction rate is too fast which leads to an incomplete reaction. As a result a lean matrix produces with more open structure which tends to crack during sintering process and impact the homogeneity of the mixture by precipitation [90, 91]. However, increasing of R value cut down the organic particles quantity in the film. Recommended molar ratio for acidic solution in R=4 [86].

Sintering Temperature: Homogeneity, porosity and purity of the silica gel are somewhat depends on the drying conditions of the mixture. At atmospheric condition, gel may shrink due to loss of water content and alcohol which initiates crack in the structure. So drying temperature and condition is an important factor after gelation. Moreover, drying at high temperature (100-500^oC) removes the organic particles from the mixture and forms Si-O-Si bond. When the thermal treatment temperature is 350^oC, porosity can reach up to 78%, i.e. high drying temperature tends to increase the porosity [86].

Dipping Speed: Substrate withdrawal speed determines the film thickness of the final deposited layer. The structure of the sol-gel thin film depends on the solvent evaporation and condensation reactions [92]. A wide range of speed variables has been tested to determine the effect of withdrawal speed on surface smoothness and optical performance as a protective layer.

5.4 SOL-GEL PREPARATION

The two-step acid catalyzed sol-gel process consisted of the following steps:

1) Mix pure tetraethylorthosilicate (TEOS), absolute ethanol (EtOH), and 0.1 M HCl solution with a molar ratio of 1:12:1 TEOS:EtOH:HCl, stirring under reflux at 60˚C for 90 minutes.
    a) This molar ratio equates to a volumetric ratio of 10 ml TEOS/ Xml EtOH/0.81 ml 0.1 M HCl.
    b) The reflux apparatus consists of a 250 ml Erlenmeyer flask, resting on a hot plate, and connected to a 300 ml chilled water condenser.
    c) Monitor the pH of the solution; it should be approximate 2.
2) Add H2O to a final H2O/TEOS molar ratio of 4:1, stirring under reflux at 40˚C for 60 minutes.
    a) Again, the pH should be around 2 during this step.
3) Dip coupons and withdraw at a constant rate of 100 mm/min.
4) Dry at 60˚C for 25 minutes.
5) Sinter in inert N2 or Ar atmosphere at 550˚C for approximately 60 minutes.

With time, condensed silica species linked together to form a 3 dimensional network which formed into gel. PH value of the final product should be maintained between 2.0-2.5 to obtain a fine, dense network.

Error! Reference source not found. shows the reflux apparatus for the sol-gel process.

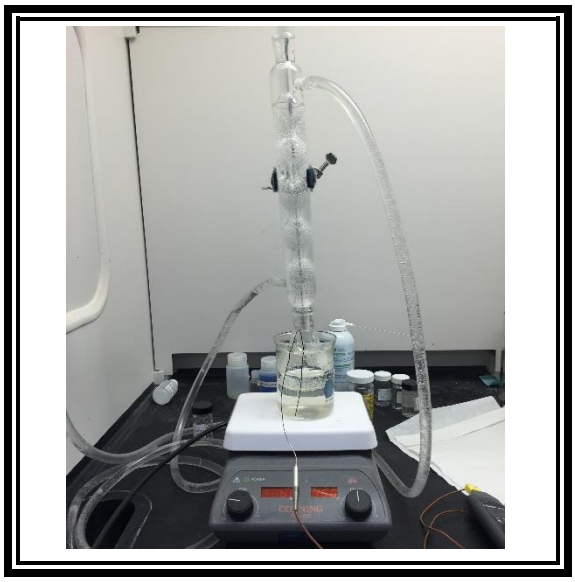

Figure 5.1: Reflux apparatus for silica sol-gel procedure

After preparing the solution, inorganic or metal organic sols are deposited on top of the metal substrate via dipping process. Substrate withdrawal speed determines the film thickness of the final deposited layer. The structure of the sol-gel thin film depends on the solvent evaporation and condensation reactions.

Experimental results are discussed with more details in chapter7.

Chapter 6: Solar Furnace Test

This chapter demonstrated the flux spreading capability based on the NBB design mechanism, and verified the surface condition, thermal fatigue, visual inspection of optical properties and the incident angle effects on the flux distribution that provide extended heat transfer area for particle heat absorption. NREL's high flux solar furnace (HFSF) testing facility

6.1 HFSF TEST SET-UP

The novelty of this conceptual NBB receiver is, this design is divided into three different optical zones; front or flare section, middle section and end section. These three sections are distinguished by their optical properties and thermal stability at temperatures. That is, flare section is highly specular surface but operable only at 150^{o}C, middle section is high hemispherical but low specular reflective surface which can thermally stable up to 1000^{o}c and the end section is an oxidized metallic surface with 95% absorptivity at 1000^{o}c.

This receiver is being tested at the National Renewable Energy Laboratory (NREL) solar furnace testing facility, Golden, CO. It was hard to control a homogenous temperature distribution throughout the exposure time when concentrated solar radiation directly applied to the sample. However a shutter engaged in front of the concentrated beam operated from control room to conduct the test. Function of this shutter were to temperature control and focus the concentrated beam to the tube axis.

Error! Reference source not found.6.1 A shows the on-sun testing set up at the HFSF, and **Error! Reference source not found.**6.2 B shows the on-going testing with applied solar flux. The entire setup was located on a XYZ table and the frame tilted to adjust the direction of the beam into the receiver. The concentrated beam of light comes into the test section at 7 degree angle. The tilting device can change the angle between the incident beam and tube axis from 0 to 22 (**Error! Reference source not found.**6.1 A and 6.1nB). The focal point of the HFSF was located at the tube aperture. Two IR cameras were put on each side of tube aiming at the tube elevation, which

record the thermal images across the tube with the solar heating process. Type K thermocouples were located at the tube entrance then 3 inches apart along the outside of the tube and one at the end cap, which is a thin stainless steel sheet placed at the back end of the tube to collect the solar flux on the tube end. The periphery outside the tube aperture was shielded with a high-temperature insulation board, such that the flux was only directed into the tube aperture, and the external sides of the tube were isolated from the solar flux.

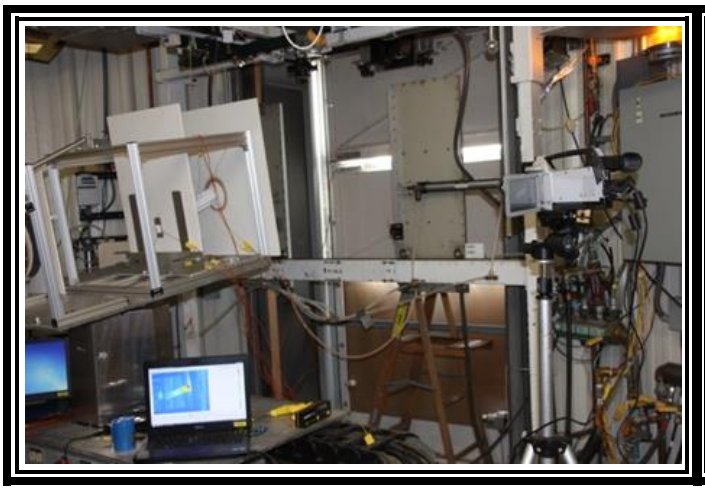

Figure 6.1 A: Side view of HFSF test setup

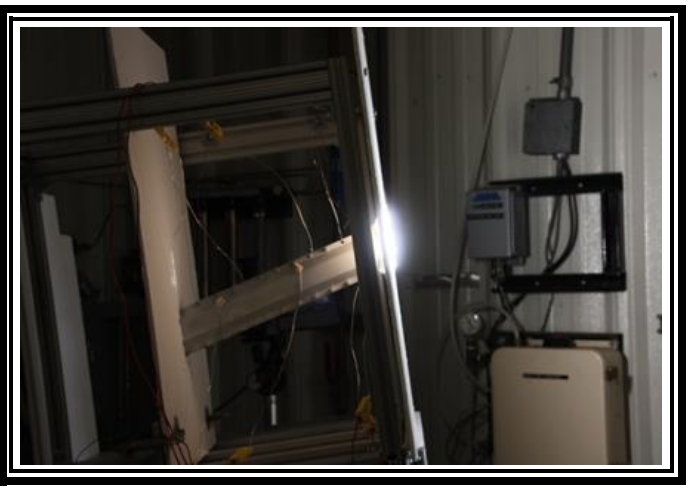

Figure 6.1 B: Tilted setup with incoming flux

6.2 TUBE FABRICATION

Three hexagonal shape absorber tubes were fabricated with different coating configuration. Each single tube was manufactured into two parts so that the coating can be easily applied in the middle section of the tube. After fabrication, both parts were assembled by joining with the screws. Figure 6.2 A is the schematic of an assembled single absorber tube and figure 6.2 B is mirror polished stainless steel single absorber tube.

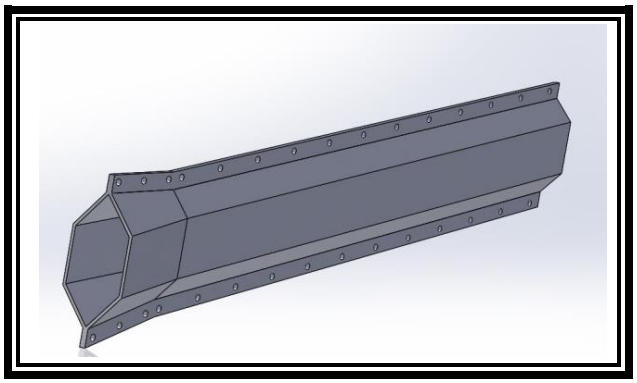

Figure 6.2 A: Schemetic of an assembled single absorber tube

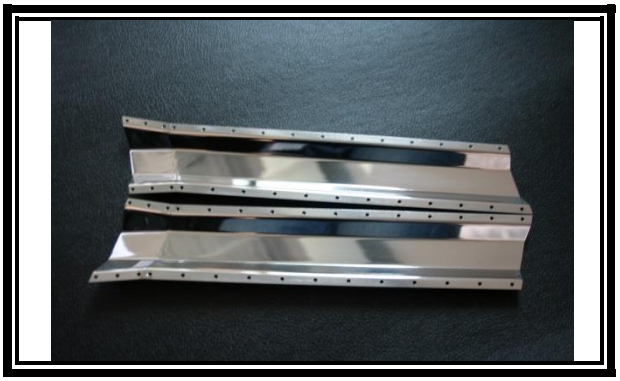

Figure 6.2 B: Mirror polished SS single tube

The first tube was just the bare tube, second one is mirror polished with 67% specular reflectivity and the third one has three different coating zone. In the third tube; front section or flare was glued with alanod (specular reflectivity 95%), middle section was sprayed with Al2O3 ceramic aerosol (hemispherical reflectivity 92%) and tube end was oxidized at 800oC. All three tubes were sprayed with white high temperature silica based ceramic coating for IR camera visualization.

6.1 SOLTRACE GEOMETRY

In SolTrace modeling, the sun shape was defined for latitude 39.50, location Golden, Colorado; 180 days in the year. Heliostat position was calculated from global coordinates' origin and aim point location for that specific day. Five system stages; heliostat, primary mirror array, attenuator, power plane and hexagonal tube were composed of number of elements to replicate the solar furnace test setup. The hexagonal tube geometry was featured with total number of 68 triangular elements.

Tube length was divided into three sections distinguished by optical properties. The front or the flare section is highly specular reflective surface, the middle section is highly diffuse reflective surface and the back part is absorptive surface. Specularity error defines surface specular or diffuse characteristics for each section. Specular properties of the flare section aimed to help penetrate

more flux and allow uniform flux spreading inside the tube. Table 1 contains detail optical properties:

Table 6.1: Optical properties of three different coating zone

Sections	Length (in)	Reflectivity	Transmissivity	Slope error (mrad)	Specularity error (mrad)
Flare	1.517	0.9250	1.0000	0.0001	200.00
Middle	5.18	0.8000	1.0000	2.0000	800.00
Back	6.303	0.1000	1.0000	2.0000	800.00

Number of rays to be traced, is a function of result accuracy. For this case, the parameter was set at 2e+6 number of ray intersections which can be generated from maximum 2e+8 sun rays. Eight processors were utilized for speed up calculation. All calculation includes sun shape and optical errors.

Numerical results are discussed with more details in chapter7.

Chapter 7: Result & Discussion

This chapter includes the experimental results of the metal surface coating reflectivity under thermal cycles at high temperature for flux spreading application on high temperature solar receiver. Numerical analysis with HSC chemistry software also predicts the material stability while it undergoes for different thermal cycles. Both experimental and numerical result shows best match with each other which validate the results. Chemical characterization of the metal coating surface after thermal cycling test, by Energy-dispersive X-ray spectroscopy (EDS) is also shown in this chapter.

7.1 FLARE SECTION COATING OF THE RECEIVER

The purpose of this work is to identify coating materials with appropriate level of specular reflectance and its corresponding methods of application on a substrate. Specular reflectance surface property is very crucial for this near black body fluidized bed cavity type receiver design performance. The coating surface with specular reflectivity ≤70% will help to improve the flux spreading inside the hexagonal tubes and uniformly distributed towards the enclosed end of the tubes. The main concern of this type of coating application is the thermal stability at temperature 150^{o}C for up to ≤10000 thermal cycle.

7.1.1 Metal coating: Thermal cycle testing

The metal coating study conducted for 3 different metals coating which are categorized into 9 different groups considering its coating thickness (Table 4.2). An Industrial partner prepared the sample material of 310 Stainless Steel (SS) coupon with dimension $1''X\ 1''\ X\ 0.060''$, one side

polished. Metal coating applied on top of 310 SS substrate with different thickness to identify the best match for desired reflective surface.

The solar weighted values for hemispherical reflectance and total specular reflectance are first measured, as shown in Figure 5.1. The hemispherical and specular values stay close to each other in the range of 60 and 90. The only exceptions are the samples coated with pure gold. They can be easily scratched and, if so, its reflective properties may change dramatically.

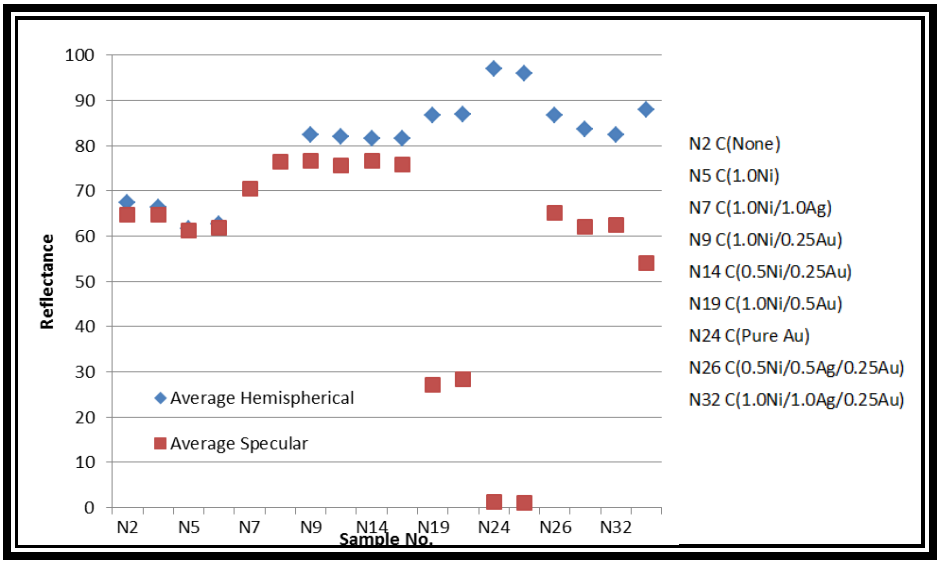

Figure 7.1: Solar weighted hemispherical and total specular reflectance for measured samples.

In the test, one sample from each group were sent into the oven for 1 hour, first, and 4 more hours, next, under the temperature of 500ºC. The coating surface changes its color even after one hour at high temperature exposure. Figure 7.2 shows picture of the tested samples before and after getting into the oven. The upper row (yellow color) is the original samples without any thermal

treatment while the bottom is the samples after one-hour thermal treatment under 500ºC. This indicates that gold is diffused into its bedding layers and the gold coating is not chemically stable.

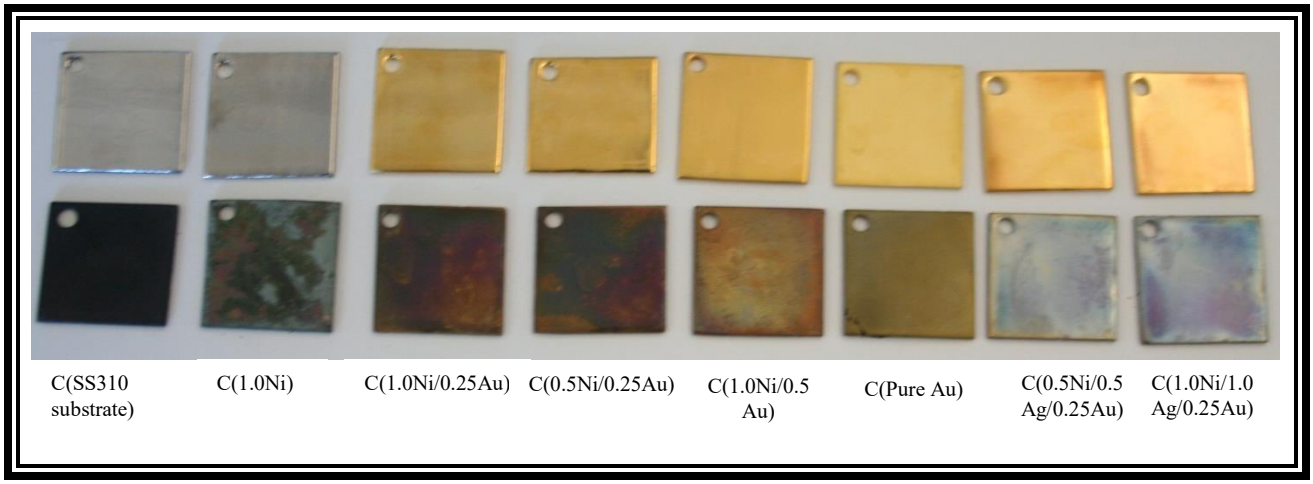

Figure 7.2: Samples before and after heat treatment at 500ºC.

The solar weighted specular reflectance is also measured for the samples under test. Figure 7.3 plots the specular value as a function of thermal cycles for the tested samples. Three time steps are chosen: initial condition, one-hour thermal treatment and five-hour thermal treatment. It can be seen that the specular reflectance decreases with increasing thermal treatment time.

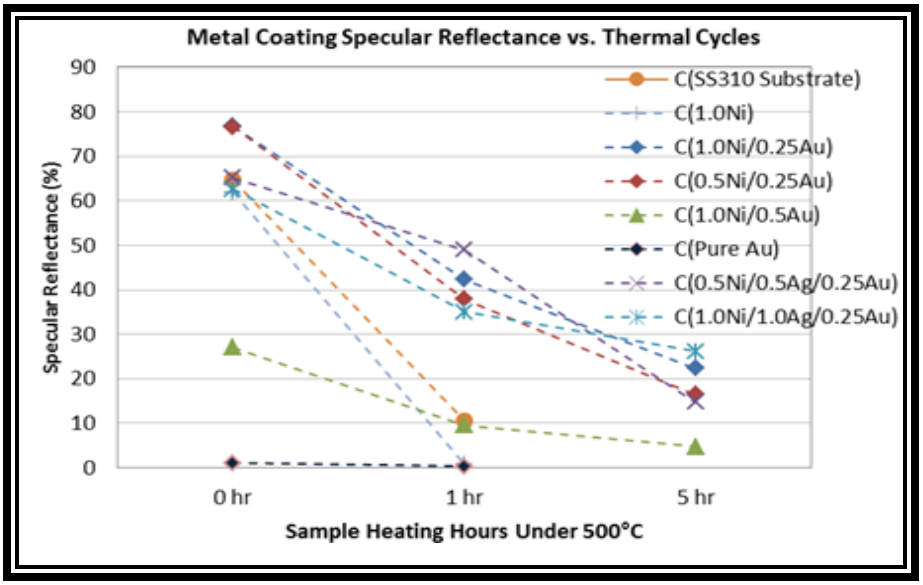

Figure 7.3: Specular reflectance as a function of thermal cycles for tested samples.

The specularity of gold-coated samples is also examined. Due to the fact that the mirror specularity cannot be measured by using the instruments at NREL, it will be derived from the specular reflectance measurements at various acceptance angles by using the D&S reflectometer (660 nm wavelength light source is used). Three solar weighted parameters required for optical characterization of a coating surface; Mirror specularity, total specular reflectance and specular reflectance as a function of temperature. To calculate the mirror specularuty a double Gaussian function $f(\varphi)$is used for four data points.

$$f(\varphi) = \frac{c}{2\pi\cdot\sigma_1^2}\, e^{-\left(\frac{\varphi}{\sqrt{2}\cdot\sigma_1}\right)^2} + \frac{1-c}{2\pi\cdot\sigma_2^2}\, e^{-\left(\frac{\varphi}{\sqrt{2}\cdot\sigma_2}\right)^2}. \tag{12}$$

Its corresponding specular reflectance becomes:

$$\rho_{spec,tot}^{660}\cdot\left(1 - \; c\cdot e^{-\left(\frac{\varphi}{\sqrt{2}\cdot\sigma_1}\right)^2} - (1-c)\cdot e^{-\left(\frac{\varphi}{\sqrt{2}\cdot\sigma_2}\right)^2}\right) = \; \rho(\varphi). \tag{13}$$

The overall RMS can then be calculated as:

$$\sigma_s \; = \sqrt{c\cdot\sigma_1^2 + \; (1-c)\cdot\sigma_2^2}\,. \tag{14}$$

For four measurements at $\varphi_i, i = 1,2,3,4$ of a mirror panel *m*, equation **Error! Reference source not found.** expands to:

$$\rho_{spec,tot}^{660,m}\cdot\left(1 - \; c\cdot e^{-\left(\frac{\varphi_i}{\sqrt{2}\cdot\sigma_1}\right)^2} - (1-c)\cdot e^{-\left(\frac{\varphi_i}{\sqrt{2}\cdot\sigma_2}\right)^2}\right) = \; \rho_{spec}^{m}(\varphi_i), i = 1,2,3,4. \tag{15}$$

The unknown coefficients $\rho_{\mathrm{spec,tot}}^{660,\mathrm{m}}$, c, σ_1, and σ_2 can be solved from the equations above. The double Gaussian fitting curves are then plotted against the raw data point. Because the number of data points is equal to the number of unknown coefficients of the fitting function, the fitting curve passes through all data points.

As shown in 7.4, a double-Gaussian function is used to fit the mirror specularity profile and its prediction on specular reflectance matches well with the actual measurement points

(marked by symbols) as a function of angular acceptance angles. It can be noted that one sample (Ni 1.0/Au 0.5) has particularly low reflectance than others.

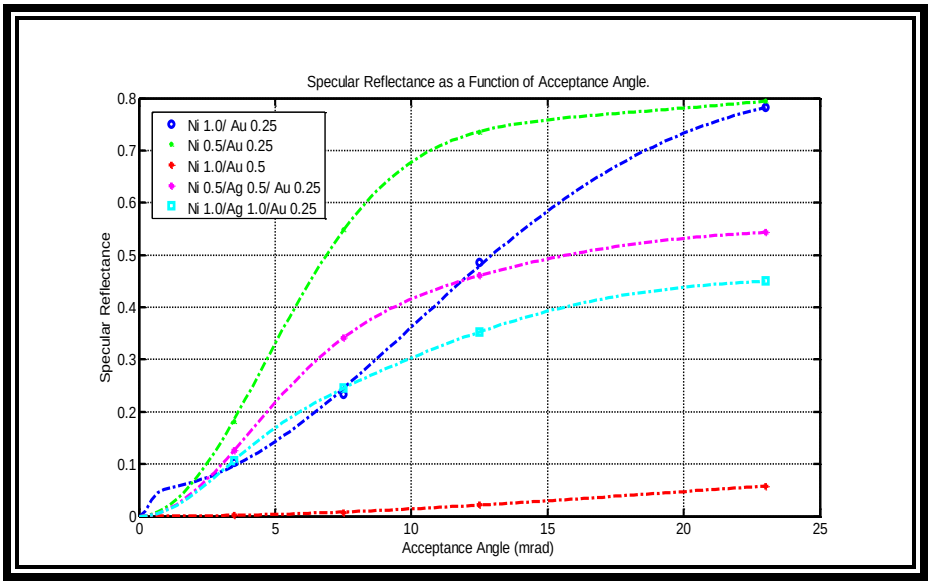

Figure 7.4: Specular reflectance fitted by double-Gaussian function.

By using the results in 7.4, the root mean square (RMS) of the mirror specularity profiles are calculated and plotted as well, as given in 7.5. The maximum value of specularity RMS is around 215 mrad and the mirror specularity RMS stays in the range of 7 mrad to 20 mrad for most types of samples.

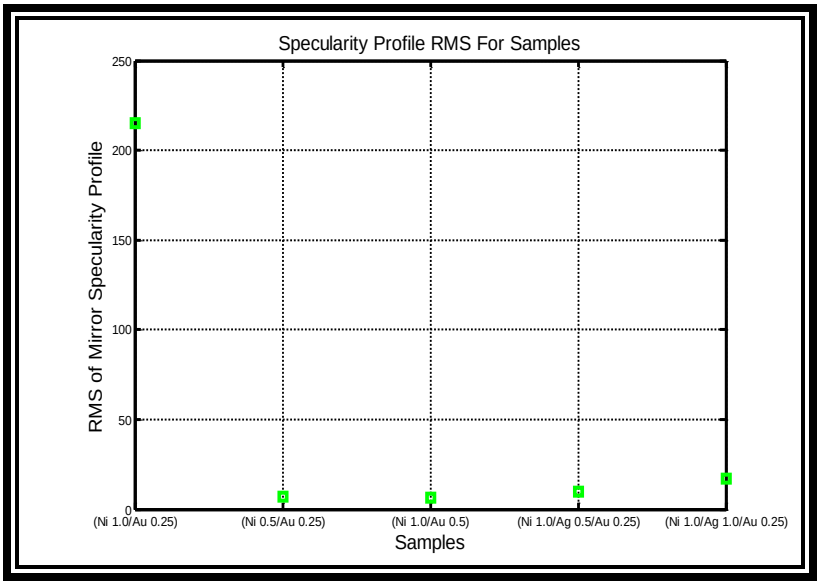

Figure 7.5: Mirror specularity profile RMS for measured sample.

EDS analysis of gold coating

The sample from Au with Ni coating showed inter-diffusion between the coating and the substrate layer. EDS analysis of the sample before and after the thermal testing confirmed this notion of inter-diffusion. Figure 5.6 shows that Au is quite stable while applied on top of 25.4 μm Ni coating by electroless coating method. But it oxidized with Ni and form nickel oxide when it undergoes thermal cycling test at 800 ºC temperature (Figure 5.7). This phenomenon reduces the surface reflectivity with elevated temperature which means, it will not meet the goal of ≤10000 thermal cycles life time period.

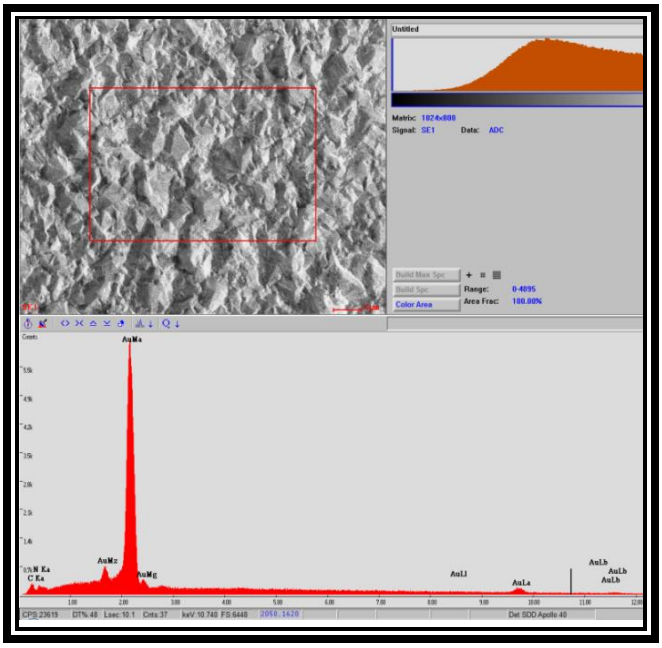

Figure 7.8: Before heating, Au is stable

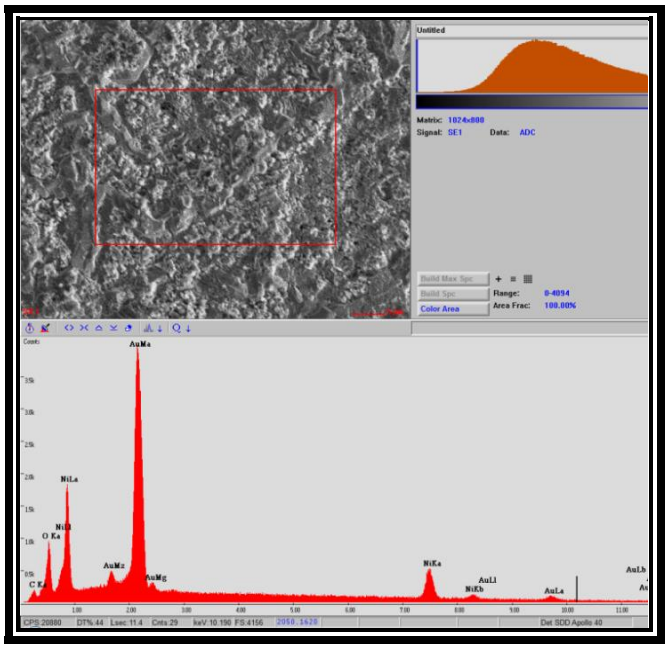

Figure 7.9: After heating, Ni oxidized at 800ºC.

7.1.2 Thermal cycle testing of Ni-Cr and Zn coating

Encouraging specular reflectance properties of Ni-Cr coating reinforce a thermal testing of this new metal coating. 1”x1” sample coupon was cut from an automotive exhaust pipe whose one side was coated with Ni-Cr and the other side was coated with Zn. The hemispherical and specular reflectance measurement is showing in table 5.1.

Table 7.1: Reflectivity measurement of Ni-Cr & Zn coating at ambient temperature

Sample	SOC-410	No. of Reading		
Ni-Cr coating		1	2	3
	Hemispherical	65.2	64.9	65.5
	Specular	61.5	61	59.8
Zn coating	Hemispherical	56	55.9	56.1
	Specular	3	2.9	2.9

The sample was set into oven for 3 hours at 800^{o}C temperature. Unfortunately this test failed after first thermal cycle. The coupon surface was completely oxidized in the presence of air at this high temperature (Figure 7.10).

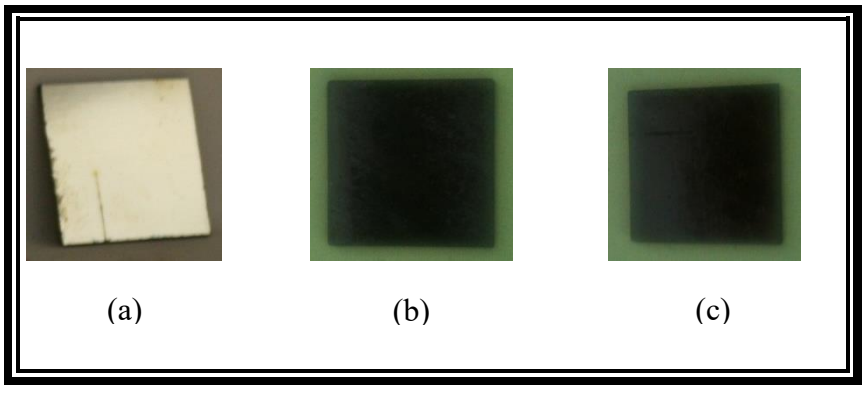

Figure 7.10: (a) Ni-Cr coating at ambient (b) Ni-Cr coating after 3 hours at 800^{o}C (c) Zn coating after 3 hours at 800^{o}C

7.1.3 Thermodynamic Modeling of Metal Coating

Thermodynamic modeling of the metal coating was conducted by chemical equilibrium software HSC chemistry. Chemical stability at high temperature range of 0-1000ºC was investigated here. The model predicts the chemical composition or inner diffusion between the coating and substrate layer at 800ºC. This result matches with the experimental data conducted in the laboratory facility.

For two different types of coating layer, the equilibrium quantities were checked with HSC modeling software. Those types are:

1. Stainless steel substrate (Fe, Ni, Cr), bond layer (Ni), the protective layer (Ag, Au), and oxygen from air
2. Stainless steel substrate (Fe, Ni, Cr), bond layer (Ni, Co, Cr, Al, Y), the protective layer (Al_2O_3), and air.

HSC software computes the possible chemical equilibrium compositions as a function of temperature ranges from 0-1000ºC. Here 0ºC means at initial condition, i.e. $\Delta G = 0$ and 1000ºC is the extreme limit. Figure 7.11 shows that, at high temperature Au is not forming any composition, whereas Ag forms silver oxides (Ag_2O, AgO_2) at >200ºC then again dissociate to form Ag at <200ºC.

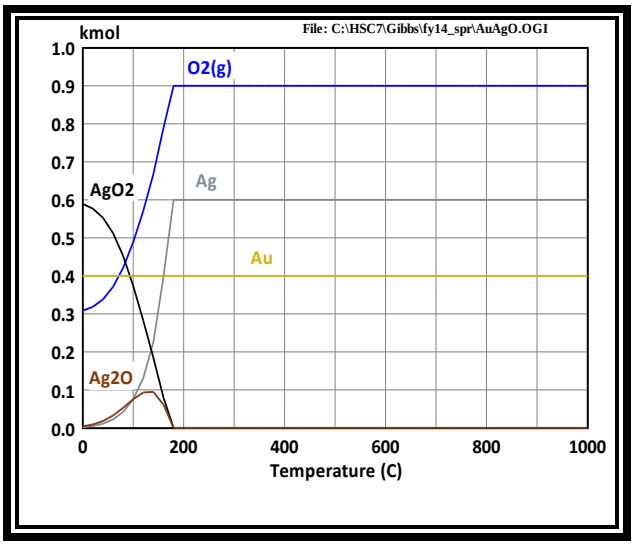

Figure 7.11: Chemical equilibrium of silver and gold with oxygen.

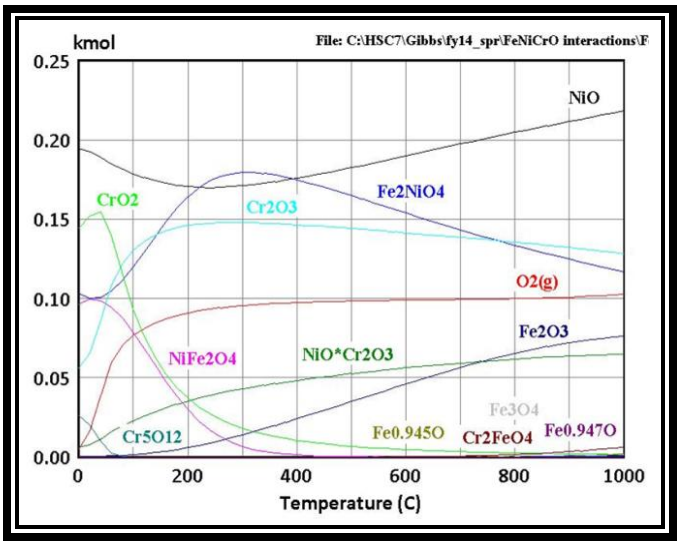

Figure 7.12: Chemical equilibrium of iron, nickel and chromium with oxygen.

Figure 7.12 spotting the metal oxides while the substrate layer interacting with the bond layer in the presence of oxygen. While operating at a temperature range from 0-1000°C; iron, nickel and chromium oxidized and forms pure and mixed metal oxide. Therefore gold/silver protective coating layer is not chemically stable at higher temperature and the specular reflectivity is diminishing as well.

7.2 THIN FILM FORMATION BY SOL-GEL PROCESS

After preparing the solution, inorganic or metal organic sols are deposited on top of the metal substrate via dipping process. Substrate withdrawal speed determines the film thickness of the final deposited layer. The structure of the sol-gel thin film depends on the solvent evaporation and condensation reactions.

Six variable speeds were tested to determine the film thickness effect on optical properties and film structure. Speed varies within a range between 200 mm/min to 5 mm/min. At higher withdrawal speed, film left a fringe when ethanol evaporates and it diminishes >50 mm/min withdrawal speed. However if the speed is >20 mm/min, substrate might have noticeable wavy

thin film formation because of comparatively more sol-gel deposition at a slow withdrawal speed. The sol-gel coating increases sample total reflectivity by 3–4%, perhaps by planarization of the reflective surface. However, the sol-gel coating reduces the specular reflectivity. If the withdraw speed is well controlled, for instance at 100 mm/min, the decrease in specular reflectivity can be less than 1% (Table 7.2).

Table 7.2: Reflectivity changes with withdrawal speed

Withdrawal Speed mm/min	Before sol-gel application		After sol-gel application		Total ref increase in %	Specular ref decrease in %
	Total Ref ρ_t(%)	Specular Ref ρ_s (%)	Total Ref ρ_t(%)	Specular Ref ρ_s (%)		
200	87.7	81.5	95.6	78.0	7.9	-3.5
150	93.2	86.1	96.7	80.0	3.5	-6.1
100	92.3	80.3	96.2	80.0	3.9	-0.3
50	93.3	86.1	96.3	83.4	3.0	-3.3
20	90.0	80.8	94.7	80.3	4.7	-0.5
5	91.7	81.2	96.0	79.3	4.3	-0.9

7.2.1 Thermal cycling test of sol-gel coated surface:

The sol-gel coated silica layer may survive high operating temperatures close to the 400°–500°C sintering temperature. However, intermetallic diffusion may occur after metal temperature exceeds 400°C; thereby, the applicable temperature for sol-gel coated reflective surface is below 400°C. The reflective surface used for the receiver heat shield is water cooled. The water is supplied from the power cycle between the condenser and the water pump. The water can be heated up to 120°C before boiling, and the heat shield maximum surface temperature should be below 150°C. In order to control water flow within the flow capacity of the power cycle and to prevent the cooling-water from boiling, the reflective surfaces on the heat shield prefer a high total reflectivity to reduce the heating load from absorption.

To satisfy this application temperature, the Ag-coated reflective samples were heated in the furnace at 150°C for 1,000 hours to test their endurance. With the improvement from sol-gel

coating, an Ag-electroplated surface obtained high total average reflectivity around 96%. After the initial heating process, the total reflectivity of those initially highly-reflective samples remained above 90% after 1,000 hrs of heating. The stability of the total reflectivity is affected by the dipping withdrawal speed and the resulting coating thickness. 1 shows the total reflectivity change with hours at temperature for different sol-gel withdrawal speeds. The optimum withdrawal speeds between 50 and 150 mm/min are consistent with the speed for improving total reflectivity.

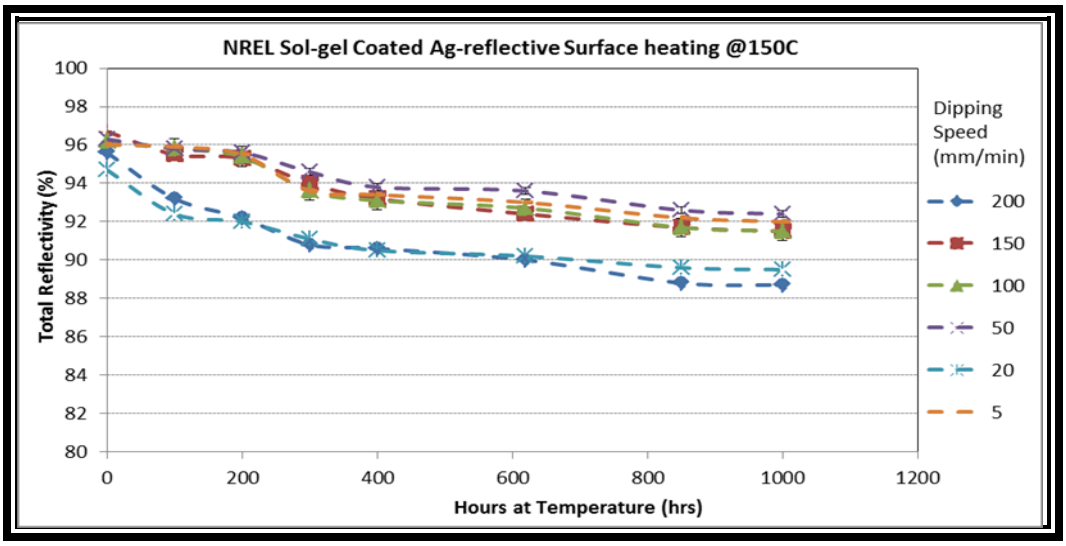

Figure 7.13. Total reflectivity change versus time for NREL sol-gel coated samples held at test temperature of 150°C

The Ag-electroplated samples recently obtained from the electroplating company were found to have inferior specular reflectivity compared to those previously obtained. We believe this resulted from poor sample packing which allowed sample surfaces to rub against one another. The poor specular reflectivity carried down to the sol-gel coated samples. Although the sol-gel coating only reduced specular reflectivity by 2%, the average initial specular reflectivity after sol-gel was ~80%, which decreases to 77% after heating as shown in Figure 7.14.

We believe that if the Ag-electroplating specular reflectivity could reach above 90% initially, and should have 85% specular reflectivity after initial heating.

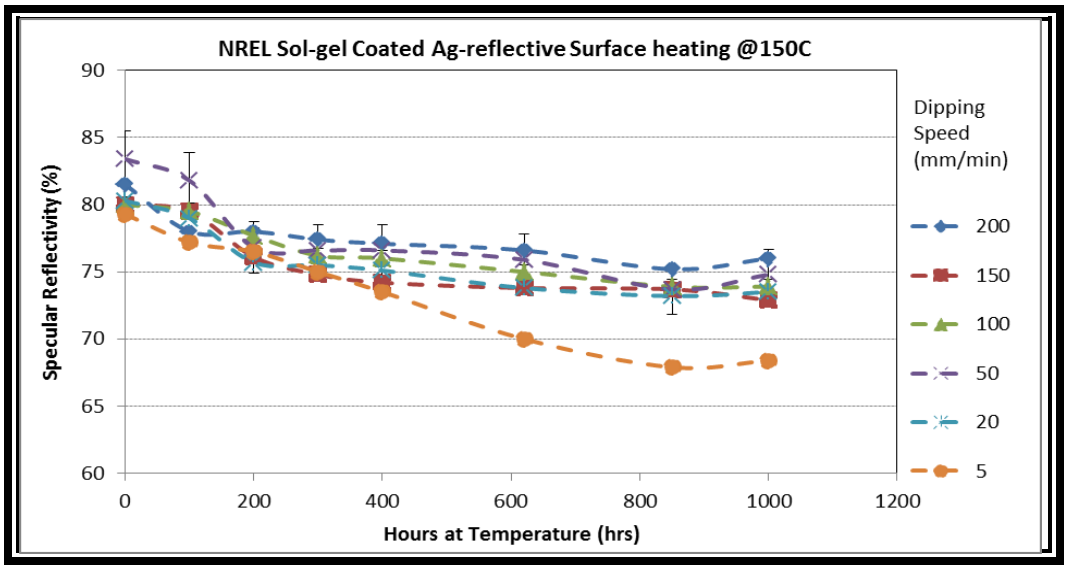

Figure 7.14. Specular reflectivity change versus time for NREL sol-gel coated samples held at test temperature of 150°C

7.2.2 SolTrace and solar furnace test result

The tested flux distribution was compared with modeled results. SolTrace modeling calculates the efficiency of the system from the ratio of total hits of sun ray on to the system to the absorbed rays into the tube. The computer codes generated data of flux distribution on the single tube geometry, and created Paraview Graphic Software files to visualize the flux spreading along the tube. Flux mapping facilitates determination of the number of thermocouples and their locations for solar furnace testing. Each case is defined upon tube inclination angle, varied from 0 degree to 20 degree. SolTrace modeled flux distributions were plotted as Paraview contours in Table 7.3 to illustrate the flux spreading for the various incident angles. The contour plots depict that flux distribution spreads from the entrance at a small incident angle, to more spreading at 10 degree angle. SolTrace result shows a preliminary indication with the on-sun testing, and the model can be further verified with refined testing and modeling. The verified SolTrace model can then

determine the input flux and tube inclination angle for prototype design and thus reduce on-sun testing risk and cost.

Table 7.3: SolTrace output for each case

Angle	SS tube w/o coating		SS polished tube		SS tube with Alanod	
	Max flux (W/m2)	Efficiency (%)	Max flux (W/m2)	Efficiency (%)	Max flux (W/m2)	Efficiency (%)
0	42260.43	91.3689	28914.32	98.7838	23204.39	88.2803
5	37790.39	91.5709	32254.58	98.6277	39263.07	89.0604
10	37828.62	91.5368	42265.94	98.4807	37370.11	89.1492
15	33404.46	91.2412	32071.32	98.7005	32258.04	88.2387
20	48952.86	90.7236	44488.25	98.8804	34620.75	86.3561

Table 7.3 explains the angular orientation effect on efficiency of a single absorber tube. The first tube, which is a bare stainless steel tube, showed 91.5709% efficiency for 5o position. The second tube with mirror polished stainless steel (specular reflectivity 67%) had maximum 98.8804% efficiency at 20o oblique position with the incident light. But, these two cases did not consider the end cap on tubes' end length, therefore simulation result and experimental result does not show a very good agreement. Third tube configuration which has three different coating regions shows best at 10o inclination angle. Then it starts to decrease in percentage, though not in a big number. This simulation exactly mimics our test case 3 and matches with the experimental result. The solar furnace testing set up different angles between the incident beam and the tube axis. The testing obtained the flux spreading for different coating conditions, and the flux penetration relating to the angles between the incident beam and the tube axis.

The significance of this first-cut on-sun testing for an absorber tube at the NREL HFSF is the validation of the NBB receiver design basis — flux spreading along the tube wall under certain incident angles between the incoming solar flux and the tube axis, and the optical properties on the tube inner surfaces. Table 7.4 lists the measured tube maximum temperature, the ratio between

the flux spreading depth and the tube aperture size, the thermal images from the infrared camera, and the flux distribution simulated from the SolTrace model under the similar geometric settings.

Table 7.4. Study of flux spreading on a 3 zone fabricated tube

0 degree	120C (In the tube front)	=~4 (2/3 tube length, end hot)	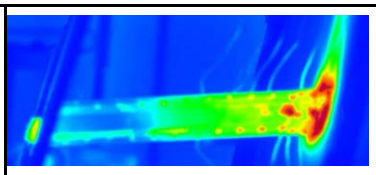	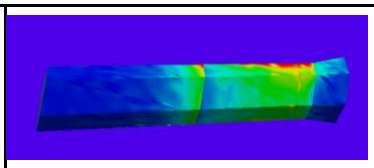
5 degree	150C (In the tube front)	=~4 (2/3 tube length, end hot)	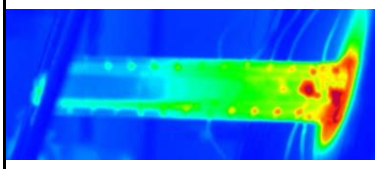	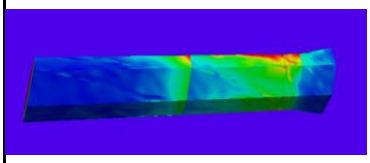
10 degree	165C	=~4 (2/3 tube length, end cool)	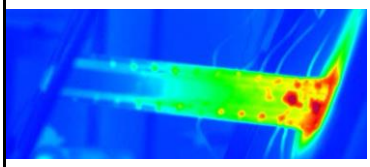	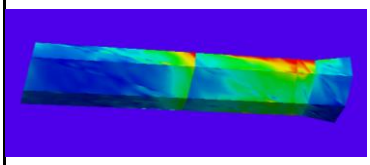
15 degree	167C	=~4 (2/3 tube length, end cool)	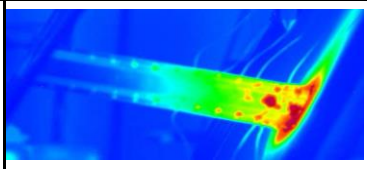	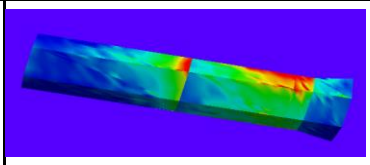
20 degree	170C	=~3 (~1/2 tube length, end cool)	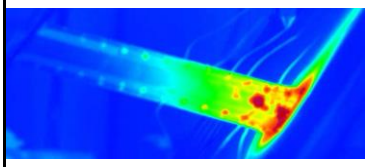	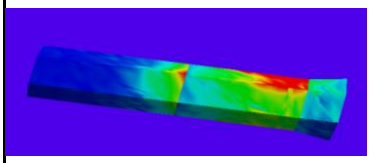

The flux distribution images in Table 7.4 shows that the 10-degree incident angle may be better than a smaller incident angle such as 0 or 5 degree. Though it looks very similar for 10 and 15 degree inclination, but 15 degree inclination angle has higher flux density on one side than other side of the tube. This result contradicts our original thought from intuitive rationale that aligned beam would penetrate deep in a tube. The discovery that a larger incident angle could get better flux spreading provides design flexibility in selecting the tube inclination angle. For the prototype

design, a smaller tilting angle can be adequate, and the small tube inclination can reduce the particle flow/heat transfer issues.

In table 7.5 column 4 represents the IR camera image done by solar furnace test and column 5 is the flux distribution image from SolTrace simulation for polished stainless steel tube fabrication. For tube tilting position <15 degree, single hexagonal tube with polished stainless steel configuration shows identical result (Table 7.5). Unlike 5 and 10 degree tube inclination angle, flux doesn't have uniform distribution through the tube when it's co-axial.

Table 7.5: Study of flux spreading on a polished stainless steel tube

0 degree	120C (In the tube front)	=~6 (whole tube length, end hot)	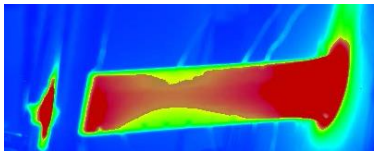	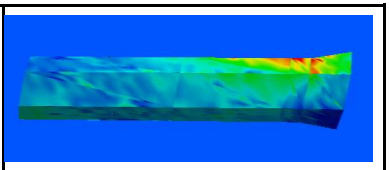
5 degree	150C (In the tube front)	=~6 (whole tube length, end hot)	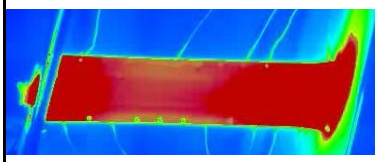	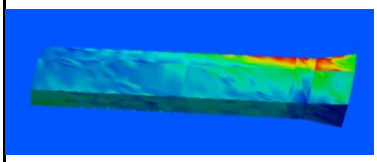
10 degree	165C	=~6 (whole tube length, end cool)	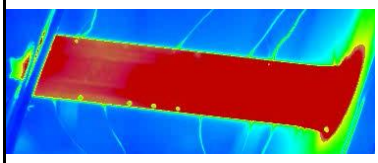	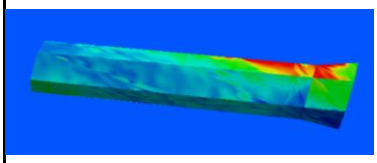
15 degree	167C	=~4 (2/3 tube length, end cool)	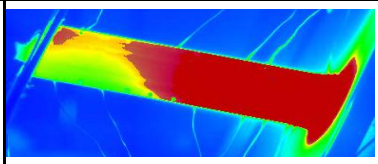	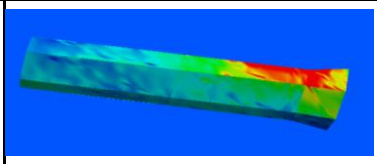
20 degree	170C	=~3 (~1/2 tube length, end cool)	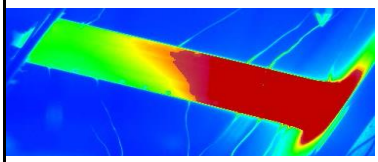	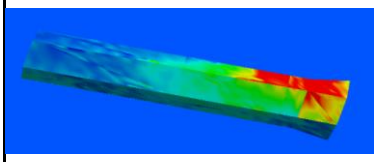

7.3 CERAMIC COATING FOR MIDDLE SECTION OF THE RECEIVER

Three types of coating methods were tested for diffusive-reflective surface, which include several off-the-shelf high-temperature paints, thermal-spray ceramic coatings (leveraging technologies developed for high-temperature thermal barrier coatings), and modified metallic surface with doped metal elements such as aluminum, chromium, chromium carbide, and nickel/chromium-based alloys. After thoroughly screening the existing coating technologies, we considered the receiver design modification that can be adapted to the tested and workable coating materials and methods such that the design can be realized and implemented in the receiver prototype fabrication and testing, and the commercial product.

7.3.1 Thermal Spray Ceramic Coating: Thermal Cycle Testing

Alumina coating was applied on top of a stainless steel substrate by thermal spray coating method with the help of Sandia National Laboratories expertise. A nickel bond coat was applied in between the Al_2O_3 coating and the substrate. The sample was cured at 600^{o}C for 1 hour. After curing, the hemispherical reflectivity and the specular reflectivity at 350 mrad (mili radian) were measured with SOC-410 at room temperature (Table 7.6).

Table 7.6: Reflectivity measurement of Al_2O_3 coating at ambient temperature

Sample	SOC-410	No. of Reading		
Al_2O_3 coating		1	2	3
	Hemispherical	72.9	73.2	73.3
	Specular	0.4	0.3	0.5

The sample was then tested for thermal cycling at 800^{o}C to observe the chemical stability and the reflective properties at high temperature environment. At first, the coupon was run into the oven for 3 hours at 800^{o}C and measured the reflectivity while cooled down. Table 7.7 presents the

new measurement where it indicates a slight increase of hemispherical reflectance, but no change in specular reflectance.

Table 7.7: Reflectivity measurement of Al_2O_3 coating at 800ºC, thermal cycle period 3hour

Sample	SOC-410	No. of Reading		
Al_2O_3 coating		1	2	3
	Hemispherical	78.5	78.5	79.0
	Specular	0.4	0.6	0.4

After successful completion of first thermal cycle test, the sample was send to the next phase for longer period of thermal cycling test. Here the test sample undergone for heating at the same temperature but for 48 hours. Ramping rate was 14 º/min and the temperature ranges from 22ºC to 800ºC. It took almost 1 hour to reach at that temperature. A K-type thermocouple was used to measure sample surface temperature. Sample was kept into the oven for 24 hours at 800ºC. After 24 hours, oven turned off and let it be cooled to room temperature. On the next day same procedure carried out and let it run for another 24 hours. After completion of 48 hours thermal cycle test, the sample initiates several cracks on the coating surface (Figure 7.15) and after a while it collapse.

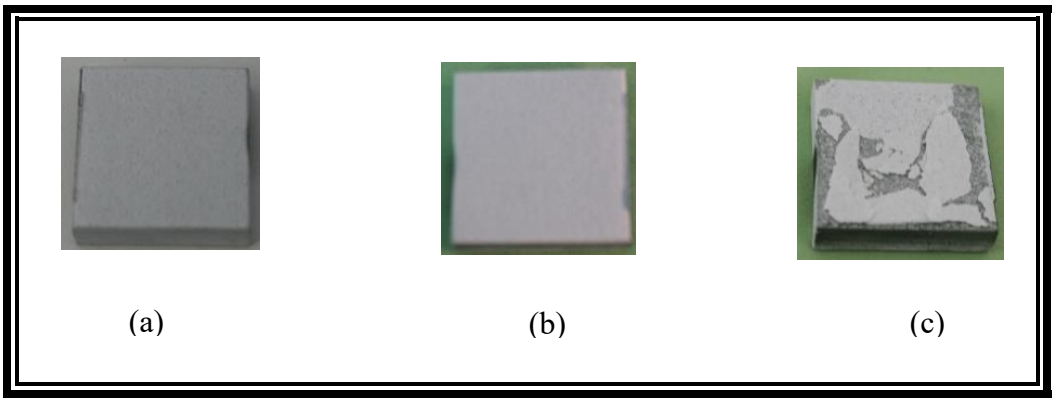

Figure 7.15: Thermal spray ceramic coating (a) Before heat treatment (b) After 3 hrs at 800ºC (c) After 48 hrs at 800ºC

Possible reason identified for this failure is, mismatch of thermal expansion coefficient between the nickel bond coat and the substrate. Thermal expansion coefficient value for stainless steel is $14 \times 10^{-6}\ /^{o}C$, Al_2O_3 $8.1 \times 10^{-6}\ /^{o}C$ and nickel bond coat $17 \times 10^{-6}\ /^{o}C$. So, there has quite difference in thermal expansion value between the bond coat and the Al_2O_3 coating layer. Therefore it initiates crack while it's cooling down to ambient temperature.

7.3.2 Aerosol Spray Ceramic Coating: Thermal Cycle Testing

Three different types of commercially available aerosol refractory paint were tested as a possible candidate of high temperature coating profile: zirconium oxide (ZrO_2), aluminum oxide refractory paint (Al_2O_3) and silica based aluminum oxide (Al_2O_3) paint. These aerosol sprays have been applied on top of a 310 ss substrate without bond coating. After applying the paint, the samples were send to oven for curing process. All the samples were then tested for 3 hours thermal cycle test at 800ºC temperature in a convection type oven. Reflectivity measurement was taken before and after the thermal cycle test. Table 7.8 shows the data for hemispherical and specular reflectivity of 3 types of coating material.

Table 7.8: Reflectivity measurement of aerosol spray coating

Aerosol spray	Before Heating		After heating at 800 ºC for 3 hours	
	Hemispherical	Specular	Hemispherical	Specular
ZrO_2	73	0.3	81.3	0.5
Al_2O_3	77.3	0.5	92.3	0.5
Silica based Al_2O_3	65.1	0.6	83.6	0.7

From the table it is noticeable that, hemispherical reflectivity has improved for all three types of coating but the specular reflectivity value is not that promising. Another concerning issue of these aerosol sprays is, after heat treatment coating surface did not well bonded with the substrate. It was behaving like loose powder while it's cooling down to ambient temperature (Figure 7.16).

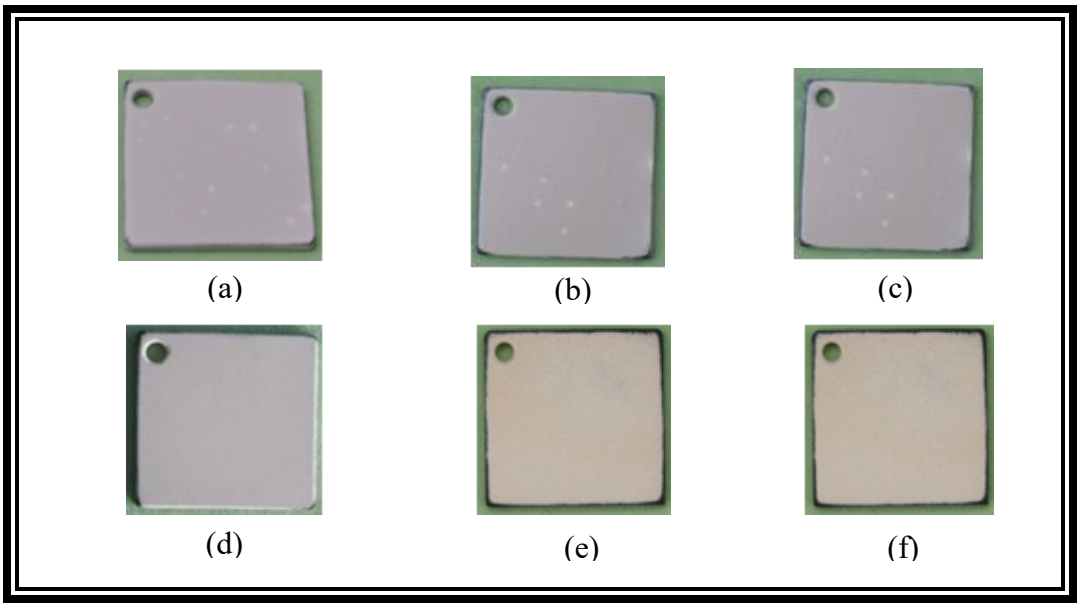

Figure 7.16: Top row; ZrO_2, Al_2O_3 & Silica based Al_2O_3 before heating, bottom row; ZrO_2, Al_2O_3 & Silica based Al_2O_3 after heating at 800ºC for 3 hour

A polished paste has been applied on top of the coating spray with the purpose of restrain loose bond between the substrate and the aerosol spray and to increase specular reflectivity. This polishing application showed at least some improvement on specular reflectivity properties and bonding behavior between the coating layer and the substrate. After applying the polishing paste on top of the silica based Al_2O_3 coating, the sample was tested for three consecutive thermal cycles at 800ºC temperature. Table 7.9 has accumulated all testing data for this test.

Table 7.9: Reflectivity measurement of silica based Al_2O_3 coating with polished surface

Reflectivity	Ambient temperature	800ºC, 24 hour	800ºC, 48 hour	800ºC, 72 hour
Hemispherical	64.8	78.8	62.4	59.9
Specular	4.0	1.1	1.1	1.0

The data analysis from table 7.9 shows that both hemispherical and specular reflectivity is decreasing with increasing number of thermal cycle.

Table 7. lists two high-temperature paints for the flux-spreading reflective surfaces. The coating methods can be applied simply by spraying, brushing, or dipping into the paint. Initial testing showed that Al_2O_3 aerosol spray coating meets the reflectivity requirement, which is >80%. After testing a few the off-the-shelf paints, the results show that none of the high-reflective paints can survive the high-temperature thermal cycling.

Table 7.10. High-temperature paints tested for thermal stability

Coating options	Coating layer and application experience	Sample pictures	Comments

Al2O3 / ZrO2 Aerosol Refractory Paint. [93]	Solar receiver up to 1,400K being tested in Weizmann Institute of Science. Diffuse surface.		Paint quality is inconsistent. Failed recent thermal test. No more efforts.
Swain Tech Engine Paint	Internal combustion engine cylinder, exhaust pipe	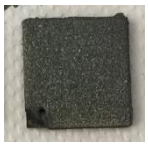	Failed the thermal test at 875˚C. Not applicable

7.3.3 Thermodynamic Modeling of Ceramic Coating

The same analysis has been done for alumina/ceramic coating with HSC chemical software. Here the modeling result of chemical stability reported that there has no chemical interaction between the coating layer and the oxygen (Figure 7.17). Alumina (Al_2O_3) doesn't react with the oxygen because alumina itself an oxide. But the nickel bond layer forms pure and mixed oxides while it's interacting with the stainless steel substrate (Figure 7.18).

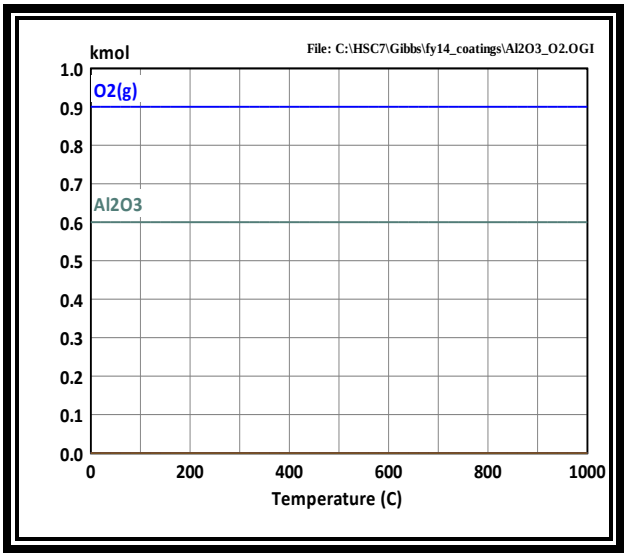

Figure 7.17: Chemical equilibrium of alumina with oxygen.

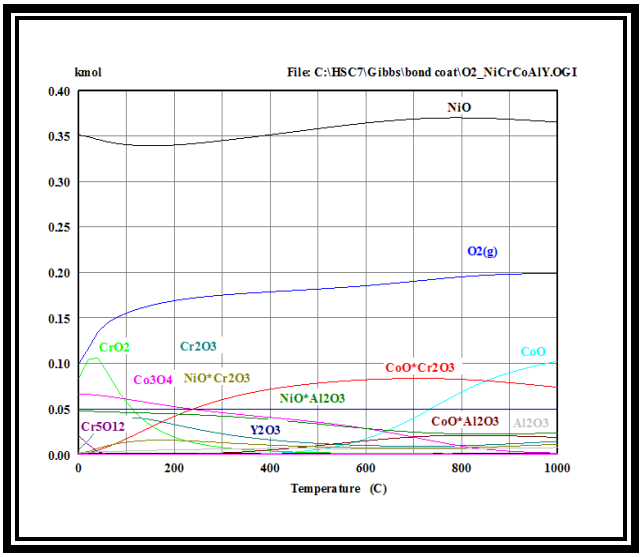

Figure 7.18: Chemical equilibrium of nickel and chromium with oxygen.

Figure 7.18 spotting the metal oxides while the substrate layer interacting with the bond layer in the presence of oxygen. While operating at a temperature range from 0-1000ºC; iron, nickel and chromium oxidized and forms pure and mixed metal oxide. Therefore gold/silver protective coating layer is not chemically stable at higher temperature and the specular reflectivity is diminishing as well.

7.4 ABSORPTIVE COATING FOR REAR SECTION OF THE RECEIVER

The rear section of the absorber tube needs to be diffusive and absorptive to capture the remaining flux prior to reaching the back wall. Several possible methods can be applied for this section including direct black oxide treatment of the stainless steel or the application of a black paint/coating. The methods are introduced below.

7.4.1 Stainless Steel Natural Oxide:

When subjected to high temperatures, the surface of unprotected stainless steel oxidizes and forms an absorptive oxide coating. The advantage of this coating is that it is easy and inexpensive to form on the surface of the stainless steel absorber tube rear section. The drawback is that it can only be formed on a receiver tube that is subjected to high temperature after the other two sections of the receiver tube have been protected from oxidation.

7.4.2 Black Oxide:

Stainless Steel can be immersed in a bath of oxidizing salts such as a sodium hydroxide-sodium nitrate solution at elevated temperature, around 120˚C for 20 minutes, to produce a black oxide coating on its surface. This oxide coating is between 150–200 μm thick and in combination with the intrinsic properties of the stainless steel substrate, makes the surface resistant to further oxidation. An advantage of this method is that it is less expensive than most other coatings/paint and can be scaled up to large batches easily. Although additional oxide will form on the stainless

steel surface at 800˚C, it should be verified that the black oxide on a high temperature stainless steel can retain the surface's black color at those temperatures.

The oxidation layer on the rear section of the tube formed in the furnace condition to meet the <12% reflectivity. This section requires highly absorptive and diffusive surface, which is easy to be obtained for stainless steel heated above 600°C. The process can be in the same step as refractory paint curing process.

The oxidation layer is consistently formed after temperature reaches 800ºC and stays black. The oxidized layer meets this performance target.

Table 1 Absorptive coating reflllecctivity over thermal cycle

Sample ID	Temperature	Hours	Total Reflectivity Reading				Average	Stdev
			1	2	3	4		
SS310-1	850	15	10.6	11.3	10.8	11.4	11.025	0.4
SS310-2	850	15	10	10.1	10	10.3	10.1	0.1
HA230-1	850	15	9.8	10.5	10.5	10.8	10.4	0.4
HA230-2	850	15	10.9	10.8	10.7	10.8	10.8	0.1

Chapter 8: Conclusion

The testing results verify the flux spreading mechanism in the NBB receiver design, and provide confidence in selecting the proper receiver-tube inclination angle. However, as a first-cut test in a tight schedule due to preparation and weather conditions, the results reported only as a rough correlation between the thermal image and the modeled flux. Although certain patterns could be identified in comparing the flux distributions from these two methods, controlled test on the prototype tube and refined SolTrace results with better graphic plotting will be improved for the prototype design verification. Sol-gel coated reflective surface can be used as a secondary concentrator for a cavity receiver in a tower CSP plant. Durability tests on sol-gel protected silver coating were performed for a variety of sol-gel coating samples. Sol-Gel coating shows good long-term stability for total reflectivity, but initial specular reflectivity needs further improvement.

Thermal-sprayed ceramic coating cannot achieve specular reflection after lapping, or grounding. Thermal-sprayed surface can have high diffuse reflectivity, and is stable for temperatures to 1000^{o}C. Ceramic sprayed coating used in high-temperature (1300^{o}C or above) may be applicable for the high-diffusive reflecting surface with proved reliability with the usage in gas turbine blade.

The rear section meets the performance target. Though very few samples were tested to make a firm decision, but literature review and experimental observation cross-match confirms that.

1. D. Arvizu, e.a., *Direct solar energy in IPCC serial report on renewable energy sources and climate change mitigation*, 2011: New York.
2. EASAC, *Concentrating solar power:its potential contribution to a sustainable energy future*, 2011, The European Academies Science Advisory Council
3. Agency, I.E., *Technology Roadmap Solar Thermal Electricity*, in *Technology Roadmap*2014.
4. Falcone, P.K., *A handbook for solar central receiver design*, 1986, Sandia National Labs., Livermore, CA (USA).
5. Tyner, C.E., J.P. Sutherland, and W.R. Gould, *Solar two: A molten salt power tower demonstration.* VDI BERICHTE, 1995. **1200**: p. 53-53.
6. Energy, D.o., *2014: The year of concentrating solar power*, May 2014.
7. Müller-Steinhagen, H. and F. Trieb, *Concentrating solar power.* A review of the technology. Ingenia Inform QR Acad Eng, 2004. **18**: p. 43-50.
8. Segal, A. and M. Epstein, *Optimized working temperatures of a solar central receiver.* Solar Energy, 2003. **75**(6): p. 503-510.
9. Ho, C.K. and B.D. Iverson, *Review of Central Receiver Designs for High-Temperature Power Cycles (Presentation)*, 2012, Sandia National Laboratories (SNL-NM), Albuquerque, NM (United States).
10. *Concentrating Solar Power*. 10/01/213; Available from: http://energy.gov/eere/sunshot/concentrating-solar-power.
11. Kolb, G.J. and R.B. Diver, *Screening analysis of solar thermochemical hydrogen concepts.* Sandia Report No. SAND2008-1900, Sandia National Laboratories, Albuquerque, NM, 2008.
12. Feher, E.G., *The supercritical thermodynamic power cycle.* Energy conversion, 1968. **8**(2): p. 85-90.
13. Wang, J., et al., *Parametric optimization design for supercritical CO 2 power cycle using genetic algorithm and artificial neural network.* Applied Energy, 2010. **87**(4): p. 1317-1324.
14. Yamaguchi, H., et al., *Solar energy powered Rankine cycle using supercritical CO 2.* Applied Thermal Engineering, 2006. **26**(17): p. 2345-2354.
15. Zhang, X. and H. Yamaguchi, *An experimental study on evacuated tube solar collector using supercritical CO 2.* Applied Thermal Engineering, 2008. **28**(10): p. 1225-1233.
16. Turchi, C.S., Z. Ma, and J. Dyreby. *Supercritical carbon dioxide power cycle configurations for use in concentrating solar power systems*. in *ASME Turbo Expo 2012: Turbine Technical Conference and Exposition*. 2012. American Society of Mechanical Engineers.
17. Martin, J. and J. Vitko Jr, *ASCUAS: a solar central receiver utilizing a solid thermal carrier*, 1982, Sandia National Labs., Livermore, CA (USA).
18. Siegel, N.P., et al., *Development and Evaluation of a Prototype Solid Particle Receiver: On-Sun Testing and Model Validation.* Journal of Solar Energy Engineering, 2010. **132**(2): p. 021008-021008.
19. Ma, Z., *Near-Blackbody Enclosed Particle-Receiver Development*, 2012, DOE EERE SETP CSP Subprogram: National Renewable Energy Laboratory (NREL).
20. Granqvist, C., *Solar energy materials.* Applied Physics A: Materials Science & Processing, 1991. **52**(2): p. 83-93.

21. Morris, V.L., *Cleaning agents and techniques for concentrating solar collectors.* Solar Energy Materials, 1980. **3**(1): p. 35-55.
22. Trieb, F., *Characterization of solar electricity import corridors from MENA to Europe: Potentials, infrastructure, and cost*, 2009, German Aerospace Center Institute of Technical Thermodynamics: Stuttgart, Germany.
23. Behar, O., A. Khellaf, and K. Mohammedi, *A review of studies on central receiver solar thermal power plants.* Renewable and Sustainable Energy Reviews, 2013. **23**: p. 12-39.
24. Radosevich, L., *Final report on the power production phase of the 10 MWe Solar Thermal Central Receiver Pilot Plant, Report No.* SAND87-8022, Sandia National Laboratories, Livermore, CA (March 1988), 1988.
25. Alpert, D.J. and G.J. Kolb, *Performance of the Solar One power plant as simulated by the SOLERGY computer code*, 1988, Sandia National Labs., Albuquerque, NM (USA).
26. Hale, M.J., *Solar Two performance evaluation*, 1999, SAE Technical Paper.
27. Singer, C., et al., *Assessment of solar power tower driven ultrasupercritical steam cycles applying tubular central receivers with varied heat transfer media.* Journal of Solar Energy Engineering, 2010. **132**(4): p. 041010.
28. Forsberg, C.W., P.F. Peterson, and H. Zhao, *High-temperature liquid-fluoride-salt closed-Brayton-cycle solar power towers.* Journal of Solar Energy Engineering, 2007. **129**(2): p. 141-146.
29. Stern, K.H., *High temperature properties and thermal decomposition of inorganic salts with oxyanions*2000: CRC press.
30. Pacheco, J.E. and S.R. Dunkin, *Assessment of molten-salt solar central-receiver freeze-up and recovery events*, 1996, Sandia National Labs., Livermore, CA (United States).
31. Kolb, G.J., et al., *Power tower technology roadmap and cost reduction plan.* SAND2011-2419, Sandia National Laboratories, Albuquerque, NM, 2011: p. 7.
32. Siegel, N., et al. *Solid Particle Receiver Flow Characerization Studies*. in *ASME 2007 Energy Sustainability Conference*. 2007. American Society of Mechanical Engineers.
33. Smith, D. *Design and Optimization of Tube-Type Receiver Panels for Molten Salt Applications*. in *ASME Solar Energy Conference, Maui, HI, April*. 1992.
34. Smith, D. and J. Chavez, *A final report on the Phase I testing of a molten-salt cavity receiver: Volume 1, A summary report*, 1988, Sandia National Labs., Albuquerque, NM (USA).
35. Drouot, L. and M. Hillairet, *The Themis program and the 2500-KW Themis solar power station at Targasonne.* Journal of Solar Energy Engineering, 1984. **106**(1): p. 83-89.
36. Schiel, W.J. and M.A. Geyer, *Testing an external sodium receiver up to heat fluxes of 2.5 MW/m 2: Results and conclusions from the IEA-SSPS high flux experiment conducted at the central receiver system of the Plataforma Solar de Almeria (Spain).* Solar Energy, 1988. **41**(3): p. 255-265.
37. Granqvist, C.G., *Solar energy materials.* 2003. **15, pp. 1789-1803**.
38. A.Ross, C.G.R., B.Karlsson, *Stainless steel solar mirrors - A material feasibility study.* 1989. **18, pp. 233-240**.
39. Morris, V.L., *Cleaning agents and techniques for concentrating solar collectors.* 1980. **3, pp. 35-55**.
40. T.Fend, B.H., G.Jorgensen, et al, *Comparative assessment of solar concentrator materials.* 2003. **74, pp. 149-155**.

41. M.Brogren, B.K., A.Ross, et al, *Analysis of the effects of outdoor and accelerated ageing on the optical properties of reflector materials for solar energy applications.* 2004. **82, pp. 491-515**.
42. A.Kribus, P.D., R.Rubin, et al., *A multistage solar receiver: The route to high temperature.* 1999. **67, pp. 3-11**.
43. Fernández-García, A., et al., *Durability of solar reflector materials for secondary concentrators used in CSP systems.* Solar Energy Materials and Solar Cells, 2014. **130**: p. 51-63.
44. Solar, A., *Alanod MIRO-SUN®*, 2010.
45. He, Z., et al., *Microstructural characterization of low dielectric silica xerogel film.* Thin Solid Films, 2004. **462**: p. 168-171.
46. Schmidt, H.K., et al., *The sol-gel process for nano-technologies: new nanocomposites with interesting optical and mechanical properties.* Journal of sol-gel science and technology, 1998. **13**(1-3): p. 397-404.
47. Evans, G., et al., *Gas-particle flow within a high temperature solar cavity receiver including radiation heat transfer.* J. Sol. Energy Eng. , 1987. **109**: p. 134–142.
48. Morales, A. and A. Duran, *Sol-Gel Protection of Front Surface Silver and Aluminum Mirrors.* Journal of Sol-Gel and Technology, 1997. **8**: p. 451-457.
49. Marzolin, C., Smith S.P., et al., *Fabrication of glass microstructures by micro-molding of sol-gel precursors.* 1998. **10**(8).
50. He, Z.W., Zhen, C.M., et al., *Micro-structural characterization of low dielectric silica xerogel film.* 2004. **462-463, p. 168-171**.
51. Schmidt, H.K., Geiter, E., et al., *The sol-gel process for nano-technologies:New nanocomposites with interesting optical and mechanical properties.* 1998. **1-3, p. 397-404**(13).
52. Coradin, T., M. Boissiere, and L. J., *Sol-gel chemistry in medical science*, 2006, Current Medicinal Chemistry.
53. Teoli, D. and L. Parisi, et al., *Wet sol-gel derived silica for controlled release of proteins.* 2006. **116, p. 295-303**.
54. Pepe, A., Galliano, P., et al., *Hybrid silica sol-gel coatings on austempered ductile iron IADI).* 2005. **59, p. 2219-2222**.
55. Wang, D., Bierwagen, G.P., *Sol-gel coatings on metals for corrosion protection.* 2009. **64, p. 327-338**.
56. Pettit, R.B., Brinker, C.J.,, *Use of sol-gel thin films in solar energy applications.* 1986. **14, p. 269-287**.
57. ANSYS, I., *ANYSYS FLUENT 13.0 User's Guide.* Canonsburg, PA, 2010.
58. Outotec, *HSC Chemistry 7.1*, 2013.
59. Wendelin, T. *SolTRACE: a new optical modeling tool for concentrating solar optics*. in *ASME 2003 International Solar Energy Conference*. 2003. American Society of Mechanical Engineers.
60. Wendelin, T., *SolTrace 2012.7.9 contents*, 2003.
61. Röger, M., et al., *Face-down solid particle receiver using recirculation.* Journal of Solar Energy Engineering, 2011. **133**(3): p. 031009.
62. Wu, W., et al., *Proof of concept test of a centrifugal particle receiver.* Energy Procedia, 2014. **49**: p. 560-568.

63. Pawlowski, L., *The science and engineering of thermal spray coatings*2008: John Wiley & Sons.
64. Davis, J.R., *Handbook of thermal spray technology*2004: ASM international.
65. Smith, R.E., *Scratch remover and polish containing oleic diethanolamide, an abrasive alumina and a bentonite*, 1990, Google Patents.
66. Torrance, K.E. and E.M. Sparrow, *Theory for off-specular reflection from roughened surfaces.* JOSA, 1967. **57**(9): p. 1105-1112.
67. Zhu, G., D. Kearney, and M. Mehos, *On characterization and measurement of average solar field mirror reflectance in utility-scale concentrating solar power plants.* Solar Energy, 2014. **99**: p. 185-202.
68. Bendt, P., et al., *Optical analysis and optimization of line focus solar collectors*, 1979, Solar Energy Research Inst., Golden, CO (USA).
69. Gee, R., et al. *An improved method for characterizing reflector specularity for parabolic trough concentrators*. in *Proceedings of Solar PACES Conference Perpignan (France)*. 2010.
70. Zhu, G. and A. Lewandowski, *A new optical evaluation approach for parabolic trough collectors: first-principle optical intercept calculation.* Journal of Solar Energy Engineering, 2012. **134**(4): p. 041005.
71. Meyen, S., *Parameters and method to evaluate the solar reflectance properties of reflector materials for concentrating solar power technology-Official SolarPACES reflectance guideline verstion 2.5.* 2013.
72. Arvesen, J.C., R.N. Griffin, and B.D. Pearson, *Determination of extraterrestrial solar spectral irradiance from a research aircraft.* Applied Optics, 1969. **8**(11): p. 2215-2232.
73. Rabl, A., *Active solar collectors and their applications*1985: Oxford University Press.
74. Corp., S.O., *410-Solar Visible/NIR Portable Reflectometer*, S.O. Corp., Editor 2009.
75. Corp., S.O., *SOC-100 HDR Hemispherical Directional Reflectometer*, S.O. Corp., Editor 2009.
76. Morales, A.D., A.;, *Sol-gel protection of front surface silver and aluminum mirrors.* Journal of Sol-Gel Science and Tech, 1997. **8**: p. 451-457.
77. Aránzazu Fernández-García, et al., *Durability of solar reflector materials for secondary concentrators used in CSP systems.* Solar Energy Materials and Solar Cells, 2014. **130**: p. 51-63.
78. Hench, L.L. and J.K. West, *The sol-gel process.* 1990. **90, p. 33-72**.
79. Milea, C.A., C. Bogatu, and A. DUŢĂ, *The influence of parameters in silica sol-gel process.* 2011. **4, p. 59-66**.
80. Prassas, M., Hench, L.L., et al., *Ultrastructure processing of ceramics, glasses and composites*1984, New York: John Wiley & Sons.
81. Iler, R.K., *The Chemistry of Silica: Solubality, Polymerization, Colloid and Surface Properties and Biochemistry of Silica*1979, New York: Wiley.
82. Brinker, C.J. and G.W. Scherer, *Sol-gel science: the physics and chemistry of sol-gel processing*2013: Academic press.
83. Aelion, R., A. Loebel, and F. Eirich, *Hydrolysis of ethyl silicate*.* Journal of the American chemical society, 1950. **72**(12): p. 5705-5712.
84. Hench, L., G. Orcel, and J. Nogues. *The Role of Chemical Additives in Sol-Gel Processing*. in *MRS Proceedings*. 1986. Cambridge Univ Press.
85. Hench, L.L. and J.K. West, *The sol-gel process.* Chemical Reviews, 1990. **90**(1): p. 33-72.

86. Milea, C., C. Bogatu, and A. Duta, *The influence of parameters in silica sol-gel process.* Bulletin of TheTransilvania University of Brasov, 2011. **4**: p. 53.
87. Musgo, J., et al., *Ammonia-catalyzed silica xerogels: Simultaneous effects of pH, synthesis temperature, and ethanol: TEOS and water: TEOS molar ratios on textural and structural properties.* Microporous and Mesoporous Materials, 2009. **118**(1): p. 280-287.
88. Fardad, M., *Catalysts and the structure of SiO2 sol-gel films.* Journal of Materials science, 2000. **35**(7): p. 1835-1841.
89. Iler, R.K., *The chemistry of silica: solubility, polymerization, colloid and surface properties, and biochemistry. 1979.* Canada: John Wiley &Sons Inc.
90. Butler, T., B. MacCraith, and C. McDonagh, *Leaching in sol–gel-derived silica films for optical pH sensing.* Journal of Non-Crystalline Solids, 1998. **224**(3): p. 249-258.
91. McDonagh, C., et al., *Characterisation of sol-gel-derived silica films.* Journal of Non-Crystalline Solids, 1996. **194**(1): p. 72-77.
92. Brinker, C., et al., *Review of sol-gel thin film formation.* Journal of Non-Crystalline Solids, 1992. **147**: p. 424-436.
93. Hischier, I., P. Poživil, and A. Steinfeld, *A Modular Ceramic Cavity-Receiver for High-Temperature High-Concentration Solar Applications.* Journal of Solar Energy Engineering, 2012. **134**(1): p. 011004.

Vita

I have finished my Bachelor of Science in Mechanical Engineering from Rajshahi University of Engineering & Technology, Rajshahi, Bangladesh in 2006. I have received my Masters of Science degree in Mechanical Engineering from University of Texas at El Paso in 2012 and then pursue my Doctor of Philosophy degree in Fall 2012. My dissertation work mainly focus on optical characterization of a high temperature material for concentrated solar power tower receiver. I had experience to work with two pioneer national laboratories; Sandia National Laboratories, Albuquerque, NM and National Renewable Energy Laboratory, Golden, CO. Currently I am working as an Instructor at University of Texas at El Paso where I teach fundamental mechanical engineering courses. This opportunity passionate me to academia career.

Permanent address: 476/D, Apt # BC3, DIT Road, Malibag,
Dhaka 1217, Bangladesh

This thesis/dissertation was typed by Samia Afrin.